Part I

Science Goals and Capabilities of IceCube

1 Introduction

The construction of neutrino telescopes is overwhelmingly motivated by the question about the origin of cosmic rays at highest energies. The cosmic world of high energies is basically a terra incognita with respect to the processes powering it, since the directional information of charged particles is lost due to deflection in cosmic magnetic fields. Source tracing (i.e. *astronomy*) is only possible by γ-rays and by neutrinos, except for protons of the highest observed energies $> 10^{19}$ eV.

The observations of gamma-ray sources extend up to tens of TeV. With large Cherenkov telescopes like Whipple (Arizona), Hegra (La Palma), Cangaroo (Australia) and Cat (France), 13 sources of TeV gamma rays have been observed. A new generation of projects – e.g. Hess for the Southern sky, Magic and Veritas for the Northern sky – with thresholds down to 20 GeV is under development. The Milagro experiment (USA) will complement the Cherenkov telescopes with their limited duty time and angular acceptance by a full Northern sky survey at a threshold of about one TeV. In its prototype version Milagrito, it already produced relevant limits (see section 4).

The second path is followed by the Auger project in Argentina which focusses to the most energetic cosmic rays and aims to detect charged particles with energies so high that their deflection in galactic magnetic fields is negligible. Auger will consist of an extended surface array of scintillation tanks combined with air fluorescence detectors.

The third way to tackle the enigma of high-energy cosmic rays is the detection of neutrinos emitted from the sources. Neutrinos do not suffer absorption when propagating through space. The range of TeV γ-rays is about 100 Mpc only, that of protons with Auger energies even less. Therefore, the topology of the far distant high energy universe may possibly investigated only with neutrinos.

Presently operating high-energy neutrino telescopes are NT-200 in Lake Baikal and Amanda at the South Pole. Two further detectors, Antares and Nestor, are under construction in the Mediterranean. These detectors differ in many aspects from existing underground neutrino telescopes. Their architecture is optimized to achieve large detection area rather than low energy threshold. They are going to be deployed in transparent "open" media like water in oceans or lakes, or deep polar ice. Neutrinos are inferred from the Cherenkov light emitted by charged secondaries produced in neutrino interactions. Photomultiplier tubes (PMTs) spanning a three-dimensional coarse grid map the Cherenkov light.

The science goals of these instruments are manifold:

- search for steady and variable sources of high energy neutrinos like e.g. Active Galactic Nuclei (AGN) or Supernova Remnants (SNR);
- search for high energy neutrinos from transient sources like Gamma Ray Bursts (GRB) or Supernova bursts;
- study of the mechanisms accelerating hadrons to highest energies by measuring the spectrum of the neutrinos from hadron decays and comparing it to the γ-rays emitted at different wavelengths;
- search for neutrinos from the decay of superheavy particles related to topological defects (TD)[1];
- search for magnetic monopoles;
- search for other exotic particles like strange quark matter;
- search for Weakly Interacting Massive Particles which may constitute dark matter;
- monitoring our Galaxy for MeV neutrinos from supernova explosions and operation within a worldwide triangulation network;
- search for unexpected phenomena.

An extensive discussion of these goals is given in the proposal "Upgrade of AMANDA-B towards AMANDA-II " which was submitted to the DESY-PRC in June 1997 (PRC 97/05 [3]). The 1997 proposal also gives an review of the status of the field in 1997, including model predictions and observations in gamma rays and charged cosmic rays. We refer the reader to the web page [1] (section 3 of the AMANDA-II proposal). A comparatively short overview is given in the IceCube proposal of the US institutions of the IceCube collaboration to NSF (Nov.1999). It is available on the web [2] and is appended to the present application to the PRC. The most recent review of high energy neutrino astrophysics can be found in [33].

This paper gives a summary of science goals and capabilities of IceCube.

[1]This so-called top-down scenario is suggestive for the explanation of highest cosmic rays since until now no astrophysical objects (e.g AGN) have been identified which are close enough that cosmic rays of more than a few 10^{19} eV could have survived on their way to us. In this scenario, high energy particles would be "born" with high energies, and not accelerated from low to high energies, as in the standard bottom-up scenarios.

Section 2 discusses the theoretical bounds for the diffuse neutrino flux which are set by energy considerations and by the normalization of the neutrino spectrum to the high energy part of the cosmic ray spectrum. These bounds will be referred to in section 4 where expected event numbers for IceCube will be calculated from Monte Carlo simulations.

Section 3 relates the expected high energy neutrino flux to the TeV gamma flux observed from point sources.

Section 4 describes the IceCube performance in the TeV-PeV range and relates it to theoretical upper bounds and model predictions for neutrinos from cosmic accelerators.

Section 5 is devoted to the EeV capabilities of IceCube.

Section 6 presents thoughts about a possible change of the default IceCube configuration at late construction stages, with the aim to improve the PeV-EeV sensitivity at the expense of TeV sensitivity. The reason is that TeV physics at that stage is going to reach certain limits set by the unavoidable backgrounds from atmospheric neutrinos.

Section 7 discusses the detection of tau neutrinos in IceCube. Since neutrinos are produced predominantly via pion decays, one expects a ratio $Q_{\nu_e} : Q_{\nu_\mu} : Q_{\nu_\tau} \sim 1:2:0$ at the source. Flavor oscillations during the flight to the Earth lead to a flux ratio $I_{\nu_e} : I_{\nu_\mu} : I_{\nu_\tau} \sim 1:1:1$, making the identification of high energy tau neutrinos an interesting challenge. CC interactions of tau neutrinos with multi-PeV energy would lead to a characteristic "double bang" signature. Section 7 describes the detection of double bang events and gives the expected event rates for various models.

Section 8 gives an overview over the science goals beside high-energy neutrino astronomy: the search for relativistic magnetic monopoles, for slowly moving, bright exotic particles, for neutrinos from WIMP annihilation, the confirmation of neutrino oscillations with high energy neutrinos, and the detection of MeV neutrinos from supernova bursts.

Section 9 summarizes the main conclusions.

2 High-Energy Neutrino Flux from Cosmic Accelerators

2.1 Energy Considerations

Models for the origin of the highest energy cosmic rays typically predict significant neutrino fluxes. A requirement on models of cosmic ray origin is that they must provide sufficient power to supply the observed energy in the galactic or extragalactic component of the cosmic radiation. The assumption that comparable amounts of energy go into high-energy neutrinos allows a model-independent estimate of the neutrino signal that may be expected.

For instance, a basic argument for supernova explosions producing the galactic cosmic rays is that they supply the right amount of power. The energy content of the cosmic radiation is

$$\rho_E = \frac{4\pi}{c} \int E\,\phi(E)\,dE \;\approx\; 10^{-12}\ \mathrm{erg/cm}^3, \tag{1}$$

where $\phi(E) = dN/dE$ is the measured local flux of cosmic rays corrected for the effect of solar modulation. In the source region the average energy density in cosmic rays is related to the average production rate per unit volume, $q(E)$, by

$$\rho_E \;=\; q(E) \times \tau_{esc}(E), \tag{2}$$

where τ_{esc} is the characteristic residence time of cosmic rays in the source region (for example the disk of the galaxy). The characteristic time, $\tau_{esc}(E)$, decreases with energy so that the observed spectrum is somewhat steeper than the source spectrum.

Given an estimate of τ_{esc} and the rate of supernova explosions, it is possible to estimate the fraction of energy of supernova explosions needed to maintain the galactic cosmic rays in steady state, assuming that supernovae provide the power, $q(E)$. Assuming a rate of three supernovae per century with a kinetic energy of 10^{51} ergs per supernova, the conclusion is that an efficiency of $\sim$ 10% for conversion of kinetic energy of supernova ejecta into relativistic cosmic rays would suffice. In the years since this coincidence was pointed out [4], a theory of cosmic-ray modified shocks with a high efficiency for particle acceleration has been developed [11].

We can apply a similar analysis of energetics to cosmic rays of extragalactic origin. The reason to focus on the high energy end of the cosmic ray spectrum in connection with high energy neutrino astronomy is that several models have been suggested as sources of ultra-high energy cosmic rays which would also be likely sources of high energy neutrinos. These include models of active galactic nuclei (AGN) and models of gamma-ray burst (GRB) sources.

In the case of galactic cosmic rays, if the production rate of neutrinos is proportional to that of cosmic rays, $q_\nu(E) = f \times q(E)$, we would expect a flux of neutrinos related to the cosmic-ray flux by

$$\phi_\nu \propto \frac{V_D}{c} \times f \times \phi_{cr}, \tag{3}$$

where f is the efficiency with which the cosmic rays interact to produce neutrinos (either in the source region or in the interstellar medium) and V_D is the velocity of diffusion of cosmic rays out of the galaxy. $V_D \sim R_{galaxy}/\tau_{esc}$ depends on the model of cosmic-ray propagation in the galaxy, but in any case $V_D \ll c$. Thus the galactic neutrino flux should be suppressed by a large factor relative to the parent cosmic rays because of their straight-line propagation out of the galaxy. For the same reason, neutrinos, like gamma-rays, would be expected to show the structure of the galactic disk.

It is generally believed that sources of the highest energy cosmic rays are extragalactic, or at least not confined to the plane of the galaxy. Indeed, there is some evidence for a transition from one particle population to another somewhere above 10^{18} eV. There is evidence for a trend from heavy toward lighter composition. Measurements of the cosmic-ray spectrum above 10^{17} eV are summarized in Fig. 1.

For a cosmological distribution of sources of ultra-high energy cosmic rays we assume initially, for the rough estimates discussed below, that

$$V_D \;\sim\; R_H/\tau_H \;\sim\; \frac{3000\,\mathrm{Mpc}}{10^{10} yrs} \;\approx\; c. \tag{4}$$

This approximation neglects evolution of the sources and assumes that the intergalactic magnetic fields are weak enough so that charged particles can reach us from distant sources

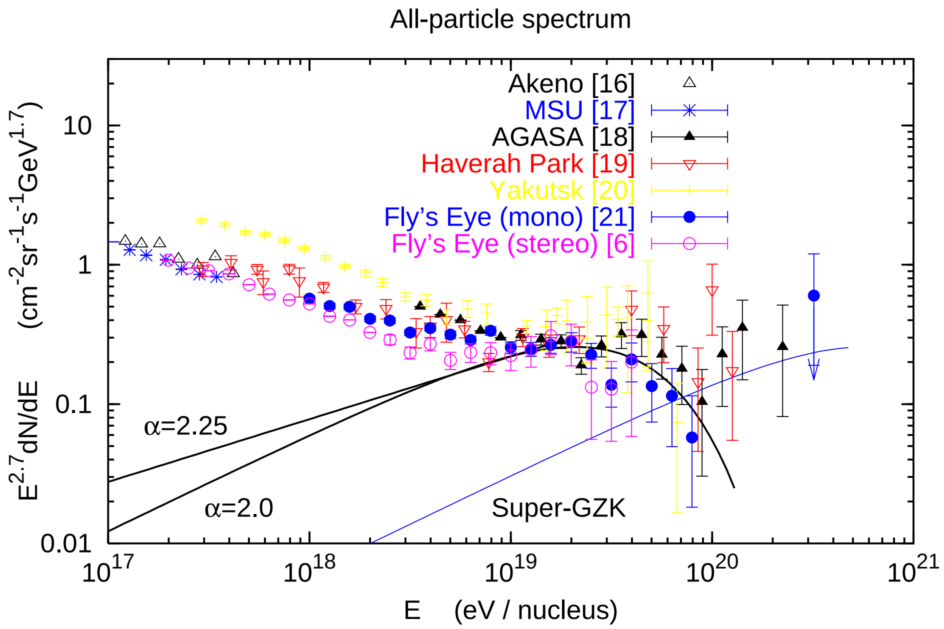

Figure 1: The high energy cosmic ray spectrum. See text for explanation of curves.

in less than the age of the universe. We will use it next to derive an estimate of the diffuse flux of high energy neutrinos that may be associated with the sources of extragalactic cosmic rays.

2.2 Normalization at high energy

Normalizing an E^{-2} differential spectrum, as is generally assumed for the sources of the highest energy cosmic rays [13, 14], to a measured spectrum with a differential spectral index close to $\alpha = 3$ is a highly uncertain operation; for a more detailed discussion, see [15]. As an example, the lower heavy line in Fig. 1 shows a spectrum with $\alpha = 2$ and an exponential cutoff at 5×10^{19} eV to represent the Greissen-Kuzmin-Zatsepin (GKZ) effect. At super GKZ energies the interaction length of cosmic rays in the microwave background is $\sim 50\,$Mpc. They therefore are unlikely to reach us from more distant sources. The excess of data above the curve for $E < 10^{19}$ eV may be attributed to the high energy tail of the galactic cosmic-ray spectrum. Integrating the energy content under this curve as in Eq. 1 gives for the energy density in cosmic rays of extragalactic origin, $\rho_{EG} \sim 2 \times 10^{-19}$ erg/cm^3. Replacing $\tau_{esc} \to \tau_H \approx 10^{10}$ yrs in Eq. 2 then leads to the estimate $q_{EG} \sim 10^{37}$ erg/Mpc^3/s. Shifting the normalization point lower (or higher) by half a decade in energy would increase (decrease) this estimate by roughly a factor of two. This is comparable to the systematic differences among the different measurements of the spectrum.

The standard technique to search for high energy neutrinos of astrophysical origin is to look for upward-moving muons induced by ν_μ that have penetrated the Earth. The signal is the convolution

$$\text{Signal} \sim \text{Area} \otimes R_\mu N_A \otimes \sigma_\nu \otimes \phi_\nu, \tag{5}$$

where R_μ is the muon range in g/cm^2 and N_A is Avogadro's number. The range and cross section both increase linearly with energy into the TeV region, after which the rate of increase slows. Neutrinos with $E_\nu < 100$ TeV are not strongly attenuated by the Earth, and much of the solid angle away from the nadir remains accessible up to 1 PeV (see also section 4). Thus the optimum range for ν_μ-induced upward muons is from a TeV to a PeV. Also in this energy range the muon energy loss is greater than minimum ionizing, which is a potential way to discriminate against the background of atmospheric neutrinos, which have a steeply falling spectrum.

Using our estimate of the energy in the extragalactic component of the cosmic ray spectrum and assuming a spectral index $\alpha \sim 2.0$ for the neutrinos as well as the cosmic rays, one predicts a neutrino event rate of $f \times 30$ events/km^2/yr [16], where f is the efficiency for production of neutrinos relative to cosmic rays. For $f = 1$ this is essentially the Waxman-Bahcall "upper bound" [13] shown in figure 2.

The "upper bound" can be evaded in multiple way, each leads to the association of larger neutrino fluxes with the sources of the extragalactic cosmic rays:

- If evolution is included, above estimate of the neutrino rate may be increased by a factor of five if sources are assumed to evolve similarly to the rate of star formation [13, 39]. This is because the ultra-high energy protons from high redshift would be attenuated by photoproduction and pair production while the neutrinos would not. Thus the neutrino flux would be greater for a given cosmic-ray flux at the normalization point.
- If the spectrum of extragalactic cosmic rays to which the normalization is made has $\alpha > 2.0$, then the corresponding estimated neutrino flux in the TeV to PeV range and the corresponding signal could also be larger.
- If the sources are not transparent (optically thick) and the cosmic rays are mostly absorbed in the source, a bound of about $10^{-6} \cdot E^{-2}$ GeV^{-1} cm^{-2} s^{-1} sr^{-1} is obtained [39]. This bound is denoted in figure 2 by $\tau_{n\gamma} \gg 1$ and is derived by demanding consistency with the diffuse gamma ray background only. As discussed in [39], even for optically thin sources ($\tau_{n\gamma} < 1$) the Waxman-Bahcall limit is exactly valid only at the normalization point of one EeV.
- If, for a class of sources, the particular sources that produce the highest energy cosmic rays are different from the ones that produce the highest neutrino fluxes. This is even expected for the case of gamma ray bursts. For instance, in the fireball model the highest energy cosmic rays are produced in sources with large Doppler factor, while those with small boost factor produce the larger neutrino fluxes.

Figure 2 illustrates the various bounds. For more details and references, see [38, 39, 37, 40, 41] The number of events in a cube kilometer detector expected from various models varies between 10 and 100 for neutrinos from GRB, and between 10 and a few thousand for neutrinos from AGN. See section 4 for predicted number of events and achievable limits.

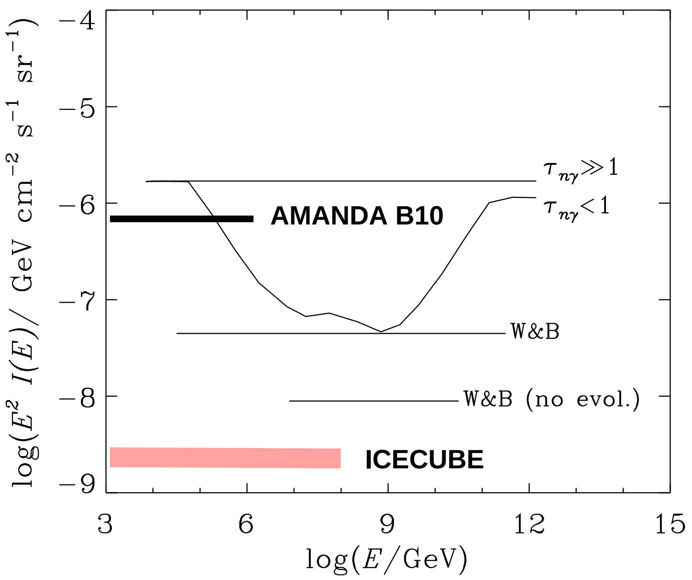

Figure 2: Cosmic ray bounds on extragalactic neutrino fluxes, The generic bound obtained by Mannheim, Protheroe and Rachen [39] for the optically thin ($\tau_{n\gamma} < 1$) and thick case ($\tau_{n\gamma} \gg 1$) are shown together with the limit inferred from Waxman and Bahcall [37] with and without source evolution. They are compared to the present Amanda limit and to the limit expected from 3 years IceCube operation.

3 High Energy Neutrino Flux from TeV Gamma-Ray Observations

The question whether the intriguing sources of TeV γ-rays such as Markarian 421, 501 are hadronic accelerators has not been answered. Although their emission may be a signature of neutral pion decay, the high energy photons can also be produced by radiative processes from accelerated electrons. Only neutrinos can present us with incontrovertible evidence of proton acceleration. High-energy neutrino astronomy has therefore the potential to discriminate between hadronic and electromagnetic origin of the TeV emission from objects such as supernova remnants, gamma-ray bursts and active galactic nuclei. With this capability, neutrino telescopes may resolve the oldest puzzle in high energy astrophysics, the origin of cosmic rays, by unambiguously identifying the acceleration to high energy of protons in the source.

As was done for the cosmic ray flux, we can use the measured TeV photon fluxes to determine the required scale of a neutrino telescope. If the observed TeV gamma rays emitted by blazars and supernova remnants are the decay products of neutral pions, one can estimate the accompanying flux of neutrinos in a largely model-independent way by assuming the production of 2 charged pions for every neutral one decaying into two photons.

Like our previous estimate using cosmic rays, also this one is subject to ambiguity when quantitatively deriving event rates. For instance, TeV photons can be the decay products of π^0's produced by accelerated protons in either pp or $p\gamma$ interactions depending on the relative target density of photons and protons in the source region where protons are accelerated [12]. The muon neutrino flux ($dN_{\nu_\mu+\bar{\nu}_\mu}/dE_\nu$) produced by the decay of charged pions in the source can be derived from the observed gamma ray flux by imposing energy conservation:

$$\int_{E_{\gamma\mathrm{min}}}^{E_{\gamma\mathrm{max}}} E_\gamma \frac{dN_\gamma}{dE_\gamma} dE_\gamma = K \int_{E_{\nu\mathrm{min}}}^{E_{\nu\mathrm{max}}} E_\nu \frac{dN_\nu}{dE_\nu} dE_\nu \tag{6}$$

where $E_{\gamma\mathrm{min}}$ ($E_{\gamma\mathrm{max}}$) is the minimum (maximum) energy of the photons that have a hadronic origin. $E_{\nu\mathrm{min}}$ and $E_{\nu\mathrm{max}}$ are the corresponding minimum and maximum energy of the neutrinos. The proportionality constant K= 1, 4 depending on whether the π^0's are of pp or $p\gamma$ origin. Important parameters in relating the neutrino flux to the gamma ray flux are the maximum and minimum energies of the produced photons and neutrinos. They appear as limits on the integrals in Eq. 6. The maximum neutrino energy is fixed by the maximum energy of the accelerated protons (E_p^{max}), and depends on whether the neutrino is produced in pp or $p\gamma$ interactions. Following our previous assumptions:

$$E_{\nu\mathrm{max}}^{pp} = \frac{1}{12} E_p^{\mathrm{max}} \quad ; \quad E_{\nu\mathrm{max}}^{p\gamma} = \frac{1}{20} E_p^{\mathrm{max}} \tag{7}$$

for the pp and $p\gamma$ case respectively. This derivation is based on the observation that $< x_F >$, the average momentum carried by the secondary pions relative to the parent proton, is $\simeq$0.2. The minimum neutrino energy is fixed by the threshold for pion production. For the pp case:

$$E_p^{\mathrm{min}} = \Gamma \; \frac{(2m_p + m_\pi)^2 - 2m_p^2}{2m_p}, \tag{8}$$

where Γ is the Lorentz factor of the accelerator relative to the observer. One has to keep in mind that in blazar jets the shocked regions where protons can be accelerated move along the jet and are therefore boosted relative to the observer. Also for $p\gamma$ interactions the minimum energy is given by the threshold for production of pions via the Δ-resonance:

$$E_p^{\mathrm{min}} = \Gamma^2 \; \frac{m_\Delta^2 - m_p^2}{4E_\gamma^{\mathrm{target}}} \tag{9}$$

Here $E_\gamma^{\mathrm{target}}$ is the typical energy of the target photons in the source which is inferred from the astronomical observations. In both cases the minimum neutrino energy is obtained from E_p^{min} using Eq. 7.

Calculation of the minimum and maximum energy of the photons is not as straightforward because high energy photons may cascade in the source reprocessing their energy. As a result they emerge as lower energy photons. In other words, the spectral index of photons can be modified by cascading and can therefore be different from the one for neutrinos. We can thus finesse the complicated details of photon cascading by treating the slope of the photon spectrum as a parameter in the energy conservation relation (Eq. 6).

High energy photons are absorbed in the interstellar infrared radiation separating the source form the telescope. Because the amount of absorption depends on the distance to the source and on the poorly known infrared background we are simply going to use as $E_{\gamma\mathrm{max}}$ the maximum observed energy, keeping in mind that this assumption leads to an underestimate of the neutrino flux.

Assuming that the photons with energies exceeding 1 TeV, we have calculated the neutrino event rates from the Crab Nebula, the supernova remnant (SNR) Cassiopeia A, the SNR-like shell Sagittarius A East and from the active galaxies Mkn 421 and Mkn 501. After converting the observed gamma ray into neutrino fluxes using Eq. 6, we calculate the event rates from Eq. 5. A sample of results is shown in Table 1; a more complete discussion can be found elsewhere[18].

Table 1: $N_{\nu_\mu+\bar{\nu}_\mu}$ events per km^2 from the Crab, Cassiopeia A, Sagittarius A East and Mkn421 in one year and from Mkn 501 during the 8 months of flaring activity in 1997. We are assuming $\alpha_\nu = 2$ for all sources except for Sgr A for which we take $\alpha_\nu = 2.1$. In the case of Mkn 421 we have used the observed flux with $E_\gamma^{\rm max} = 7$ TeV given by HEGRA. $E_{\gamma\rm min}$ and $E_{\nu\rm min}$ are expressed in GeV. The expected event rate of atmospheric neutrinos (assuming Volkova's flux [19]) in a $1^\circ \times 1^\circ$ bin on the sky is also shown for the same period of time taking into account the nadir angle of the source. The last row is the Poisson probability of observing a background of atmospheric neutrino events equal to the total signal.

Source	Crab	Crab	Cas A	Cas A	Sgr A	Sgr A	Mkn 421	Mkn 421	Mkn 501	Mkn 501
$E_{\gamma\rm min}$	1	10^3	1	10^3	1	10^3	1	10^3	1	10^3
$E_{\nu\rm min}$	400	400	400	400	400	400	$8 \cdot 10^6$	$8 \cdot 10^6$	$8 \cdot 10^6$	$8 \cdot 10^6$
$N_{\nu_\mu+\bar{\nu}_\mu}$	40	2	1.5	0.3	243	1.3	3.3	0.06	2.0	0.8
$N^{\rm atm}_{\nu_\mu+\bar{\nu}_\mu}$	3.2	3.2	1.9	1.9	2.8	2.8	2.4	2.4	2.3	2.3
Poisson	$4 \cdot 10^{-33}$	0.14	0.22	0.3	~ 0	0.17	$1.8 \cdot 10^{-2}$	0.4	0.15	0.24

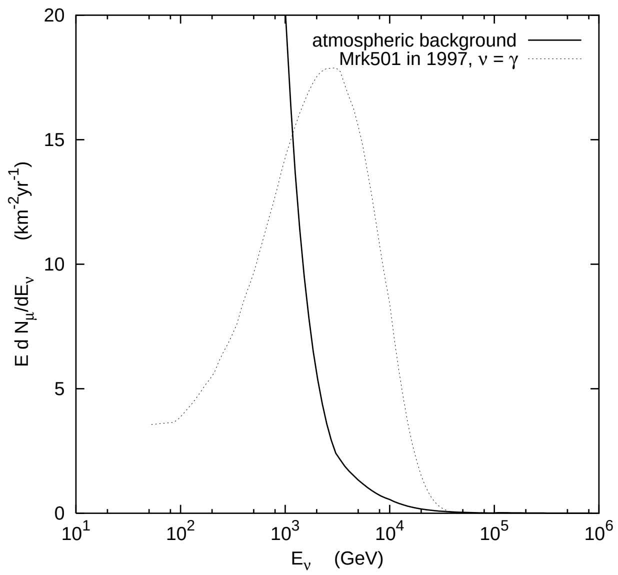

Figure 3: Signal that would be generated by a neutrino flux normalized to the level of TeV gamma emission during the extended high-state of Markarian 501 in 1997.

Inspection of Table 1 strongly suggests that elucidating the physics at the origin of TeV-photons requires a $1\,\mathrm{km}^2$ neutrino detector. Obviously, the observed TeV gamma-rays may not be of hadronic origin – data mostly suggest that they are not. Then we are left with the scaling argument based on the highest energy cosmic rays. Nature *does* accelerate hadrons to energies exceeding 10^8 TeV, and, whatever the site, the arguments presented here are likely to be approximately valid.

As another example, we show in figure 3 (taken from [15]) the signal that would be generated by a neutrino flux normalized to the level of TeV gamma emission during the extended high-state of Markarian 501 in 1997 (which is again flaring since December 2000). With $\nu/\gamma = 1$, the integral shown in the figure would give ~ 30 events per year above atmospheric background. For details and references, see "IceCube Constraints on the Hadronic Origin of the TeV Photons produced by Supernova Remnants and Active Galactic Nuclei" [2].

4 IceCube Performance in the TeV-PeV range

We have investigated the physics performance of the IceCube detector for different configurations, starting from the default configuration (125 m string distance, 16 m vertical spacing) and going into the direction of both smaller and larger spacing [46]. Early results on similar IceCube simulations have been presented in [34, 35]. Whereas in in [46] only configurations with about 5000 OMs and equidistant spacing are considered, [34, 35] cover also options with twice or half the number of OMs, and nested configurations.

The basic pattern is shown in figure 4. Apart from the triangular pattern, we also simulated rectangular patterns, which yield similar results. The circle in figure 4 indicates an area of one square kilometer. The configuration includes 80 strings and 60 OMs per string. For a vertical spacing of 16 m, this results in an instrumented length of 944 m. The top layer of OMs was assumed to be at a depth of 1400 m. Table 2 summarizes the studied configurations.

Table 2: Simulated configurations. Columns indicate different string spacings, lines different spacings of OMs along a string.

vertical / horizontal	100 m	125 m	150 m	175 m
12 m	X	X	X	-
16 m	X	X	X	-
20 m	X	X	X	X

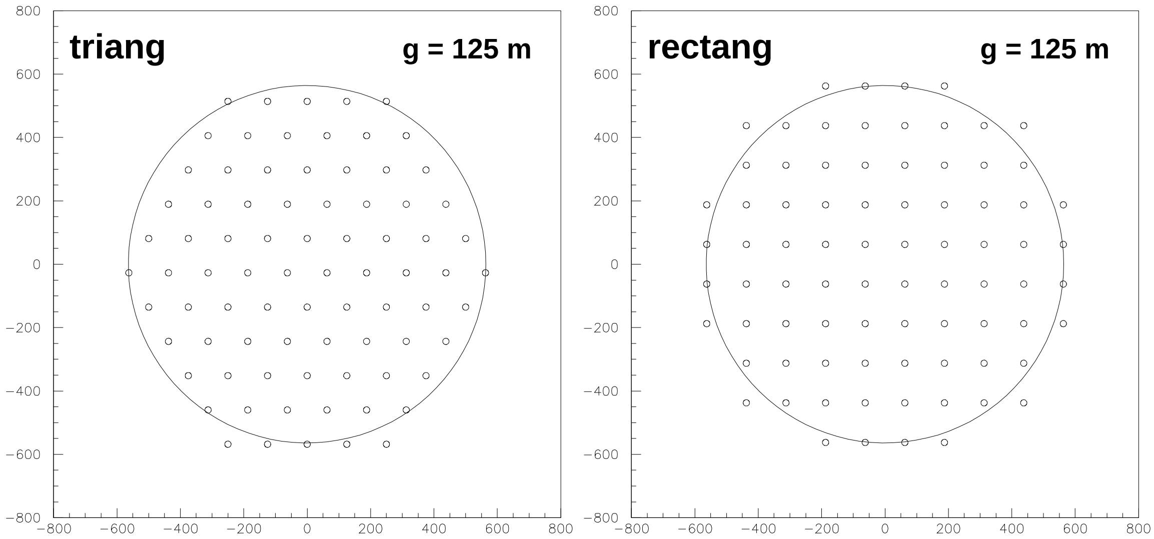

Figure 4: Top view of the two principal strings patterns investigated in this work. *left:* triangular pattern, *right:* rectangular pattern (both shown for a string spacing of 125 m). Scales are in meters.

We have simulated muon tracks generated in interactions of atmospheric neutrinos and of extraterrestrial neutrinos from Active Galactic Nuclei (AGN), with an $E_\nu^{-3.7}$ spectrum for atmospheric neutrinos and an E_ν^{-2} spectrum for AGN neutrinos. The absorption of neutrinos in the Earth is taken into account. Figure 5 demonstrates the Earth absorption. For energies below a few tens of TeV, the full lower hemisphere is visible, whereas ar energies above a few PeV the angular acceptance is reduced to zenith angles smaller than 30 degrees below horizon.

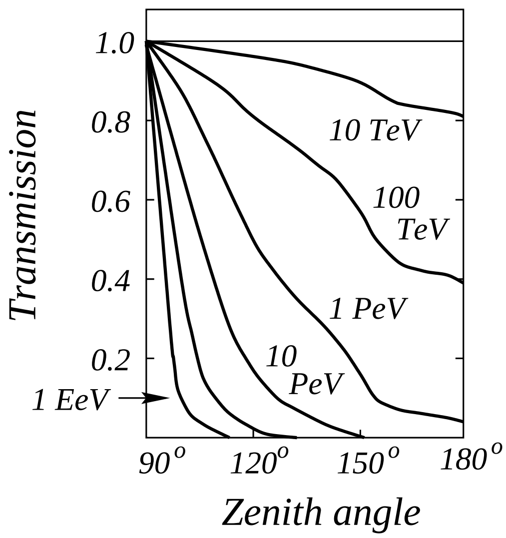

Figure 5: Transmission coefficient of the Earth for different energies as a function of zenith angle [36].

Neutrinos have been generated up to a maximum energy of 100 PeV which was set by technical limitations. Eight million events from downward muons which constitute the main source of background have been simulated and are used to demonstrate efficient background rejection. Muons were propagated with full simulation of stochastic energy loss. The detector simulation was performed with the AMANDA simulation package `amasim`. Inhomogenities of the ice have been neglected. We simulated PMTs of 10 inch diameter but did not take into aacount the possible increase in light collection efficiency due to wavelength shifter. The noise of the PMTs has been conservatively assumed to be 500 Hz (i.e. higher than the design goal of 300 Hz). A trigger was defined by the condition of at least 5 hits in a local coincidence. A local coincidence is defined with respect to the four nearest neighbors, and for a time window of 1 μsec.

The reconstruction was done in several steps using the AMANDA reconstruction package `recoos`. The start values for the full fit are obtained from two simple fast approximations called line-fit and dipole-fit (see [58] for details). As a first reduction step with respect to downward going muons, relatively weak cuts on the zenith angle obtained from these fast approximations have been applied. These cuts have passing rates of 0.91, 0.78 and 0.04 with respect to the sample from AGN neutrinos, atmospheric neutrinos and downward muons, respectively.

Next, a full likelihood fit was performed (see [57] and [58]). This fit yields a series of parameters which can be used for selecting events with high quality reconstruction and for further reduction of background. The chosen cuts are the following:

- zenith angle θ obtained from the likelihood fit is larger than 85 degrees, and $-\log L < 10$, where L is the likehood,
- ≥ 5 hits with a time residual between -15 nsec and +150 nsec ("direct hits", where the photon did not undergo many scattering acts),
- length of the projection of the direct-hit OMs to the reconstructed track is larger than 150 m,
- difference between the zenith angles obtained from line fit and likelihood fit is smaller than 10 degrees,
- the absolute value of the *smoothness*, should be smaller than 0.5. (The smoothness S measures the homogenity of the distribution of hits along the track. Exact equidistance of hits would give $S = 0$, all hits at the starting point of the track $S = +1$ and all hits at the endpoint $S = -1$.)

Figure 6 shows the energy spectra after *a)* trigger, *b)* the 3 cuts on the zenith angles obtained from line fit, dipole fit, and likelihood fit, and *c)* the remaining four quality cuts.

Results are shown for the "standard configuration" (triangular pattern, 16 m/125 m). Numbers at the top corner give the number of events and the passing rates. For AGN neutrinos, a flux of $10^{-7} \cdot E^{-2}$ GeV^{-1} cm^{-2} s^{-1} sr^{-1} has been assumed, resulting in 4265 events. The assumed flux is about a tenth of the MPR-limit and twice the WB-limit shown in figure 2.

Note that the listed standard cuts result in a passing rate of 53 % for AGN neutrinos and reduce the background from downward muons to $3 \cdot 10^{-6}$. As shown in figure 7, this background is concentrated close to the horizon. It can be easily rejected by a further zenith cut (if lower energies should be accepted), or by cuts on the number of channels (if one focuses to the separation of higher energies). Apart from the distributions for AGN neutrinos atmospheric neutrinos and the background due to muons from a single air shower figure 7 shows also the background from uncorrelated, accidentally coinciding air showers (bottom right). Uncorrelated air showers can result in two hit clusters, the earlier at the bottom and the later at the top of the array. Such events are not rejected by a simple angular cut, giving the relatively high passing rate after angular cuts compared to muons from single air showers. However, these events are easily identified by the subsequent cuts, in particular the cut on the smoothness.

The two following tables give the number of triggered and accepted events per year for the various configurations. Numbers in Table 3 are for AGN neutrinos, again assuming a flux of $10^{-7} \cdot E^{-2}$ GeV^{-1} cm^{-2} s^{-1} sr^{-1}. Table 4 gives results for atmospheric neutrinos. The upper numbers refer to triggered events, the lower numbers (in italics) to events after reconstruction and quality cuts.

Table 3: Number of triggered and accepted events per year AGN neutrinos (in thousands) assuming a flux of $10^{-7} \cdot E^{-2}$ GeV^{-1} cm^{-2} s^{-1} sr^{-1}. The upper numbers refer to triggered events, the lower numbers in italics to the events after quality cuts.

vertical/horizontal	100 m	125 m	150 m	175 m
12 m	2.9 k	3.6 k	4.3 k	-
	1.5 k	*1.8 k*	*2.2 k*	-
16 m	3.4 k	4.3 k	5.5 k	-
	1.9 k	*2.3 k*	*2.5 k*	-
20 m	4.0 k	4.9 k	5.7 k	6.5 k
	2.1 k	*2.4 k*	*2.6 k*	*2.8 k*

Table 4: Number of triggered and accepted events per year for atmospheric neutrinos (in thousands). The upper numbers refer to triggered events, the lower numbers in italics to the events after quality cuts.

vertical/horizontal	100 m	125 m	150 m	175 m
12 m	600 k	620 k	640 k	-
	140 k	*130 k*	*120 k*	-
16 m	590 k	600 k	620 k	-
	140 k	*130 k*	*110 k*	-
20 m	580 k	590 k	600 k	560 k
	140 k	*110 k*	*90 k*	*60 k*

Clearly, larger spacing is preferable for the AGN case but tends to suppress more atmospheric neutrinos after quality cuts. Going from 125 m string spacing to 150 m gives a 10% increase in accepted AGN events. The rectangular configuration gives a 5% increase in events rate. Decreasing the spacing to 12 m/100 m gives 30% loss in AGN neutrinos, but a slight increase for atmospheric neutrinos. The angular resolution for all configurations is between 0.95 and 1.05 degrees.

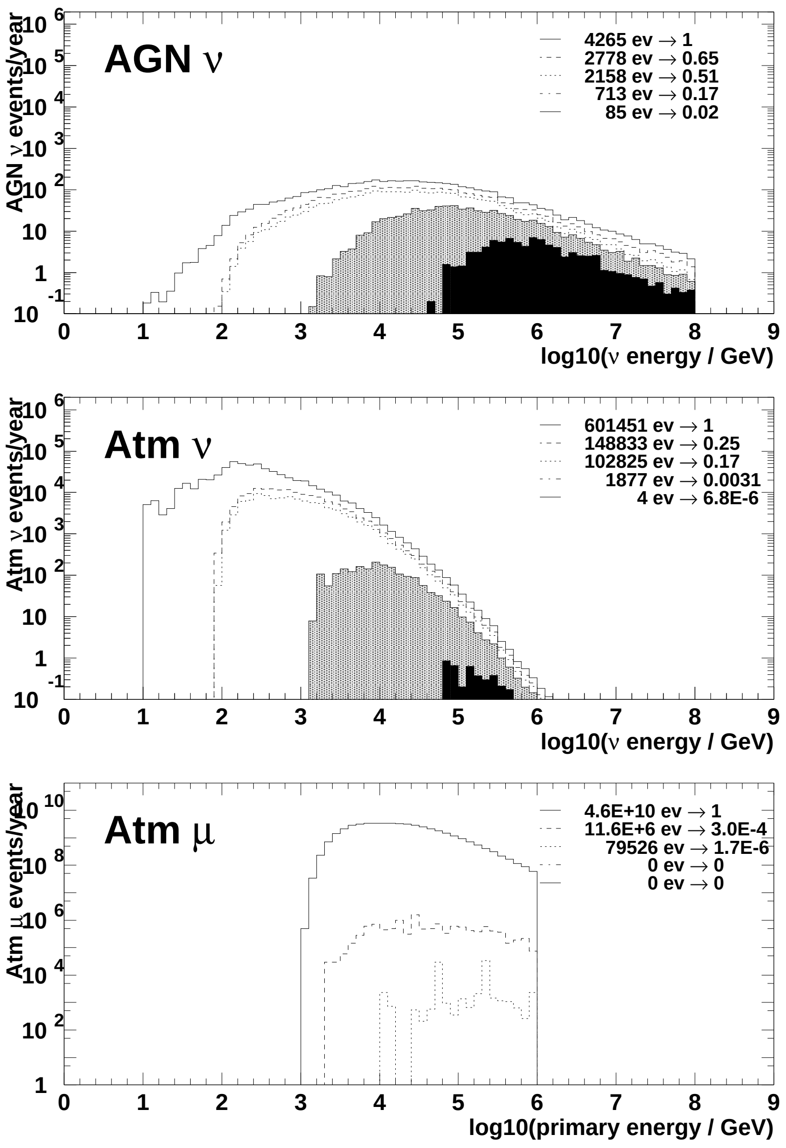

Figure 6: Energy spectra after trigger (full upper line), and the 3 cuts on the zenith angles (dashed line), the remaining four quality cuts (dotted line). The shadowed histogram gives the energy spectrum after an additional cut on the number of hit PMTs at $N_{ch} > 50$. The black histogram corresponds to a cut at $N_{ch} > 180$ and is explained in section 4. See text for further explanations.

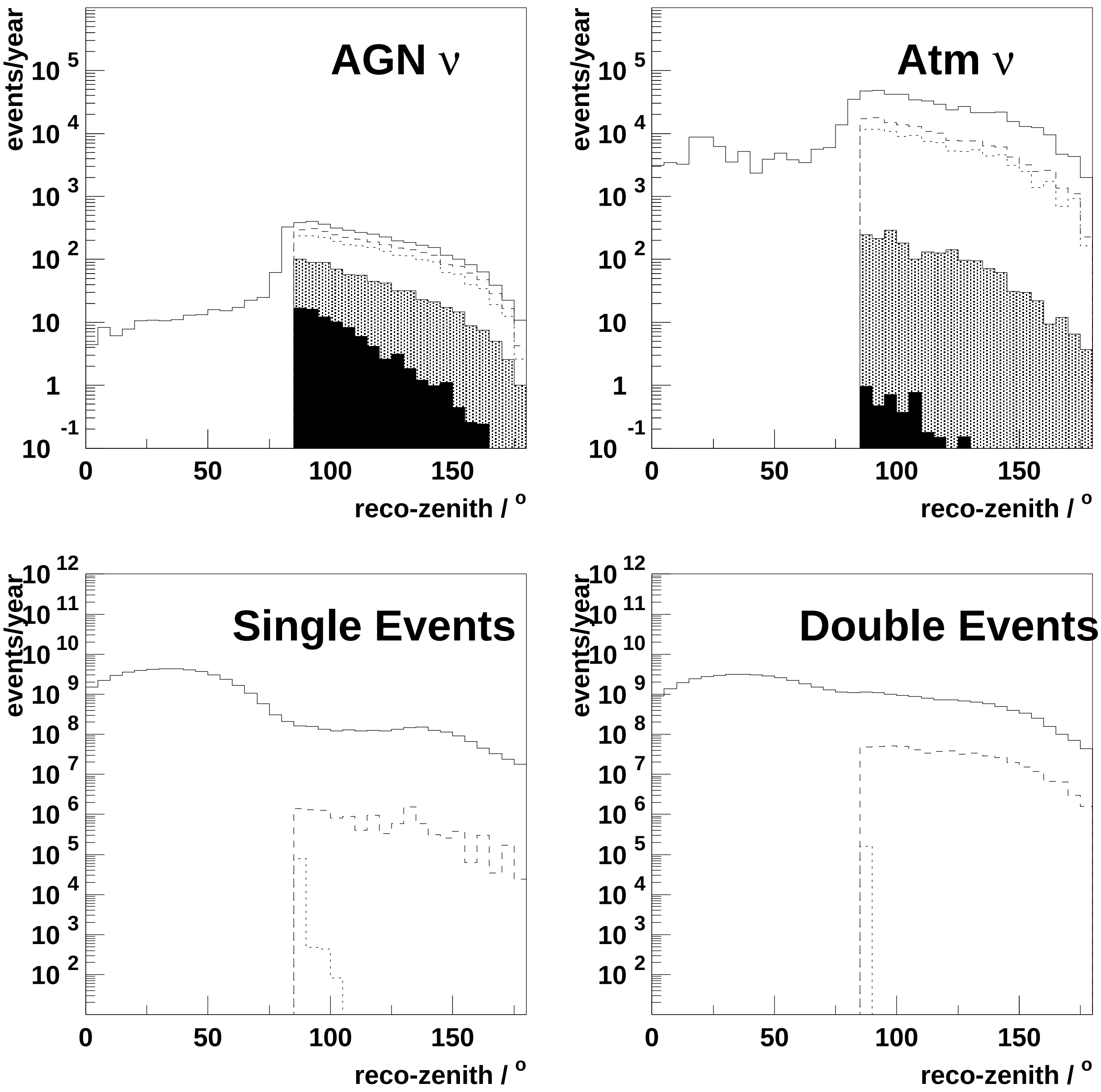

Figure 7: Distribution of the reconstructed zenith angle after trigger (full upper line), and the 3 cuts on the zenith angles (dashed line), the remaining four quality cuts (dotted line). The dashed-dotted histogram gives the energy spectrum after an additional cut on the number of hit PMTs at $N_{ch} > 50$. The dark histogram corresponds to a cut at $N_{ch} > 180$ and is explained in section 4. The bottom histograms show the background expected from single air showers (left) and from accidentally coinciding air showers (right). Note that neutrinos have been generated only between 80 and 180 degrees, therefore the cut-off at 80 degrees after quality cuts.

4.1 Achievable limits on the flux of extraterrestrial neutrinos

The theoretical bounds obtained from the normalization of neutrino fluxes to the cosmic ray spectrum and the background of diffuse gamma rays vary between $5 \cdot 10^{-8} \cdot E^{-2}$ [37] and $10^{-6} \cdot E^{-2}$ [39], both in units of $\mathrm{GeV}^{-1}\,\mathrm{cm}^{-2}\,\mathrm{s}^{-1}\,\mathrm{sr}^{-1}$. Figure 8, taken from [33], summarizes various upper bounds and model predictions. The Waxman-Bahcall (WB) bound would be a horizontal line touching the curved upper boundary.

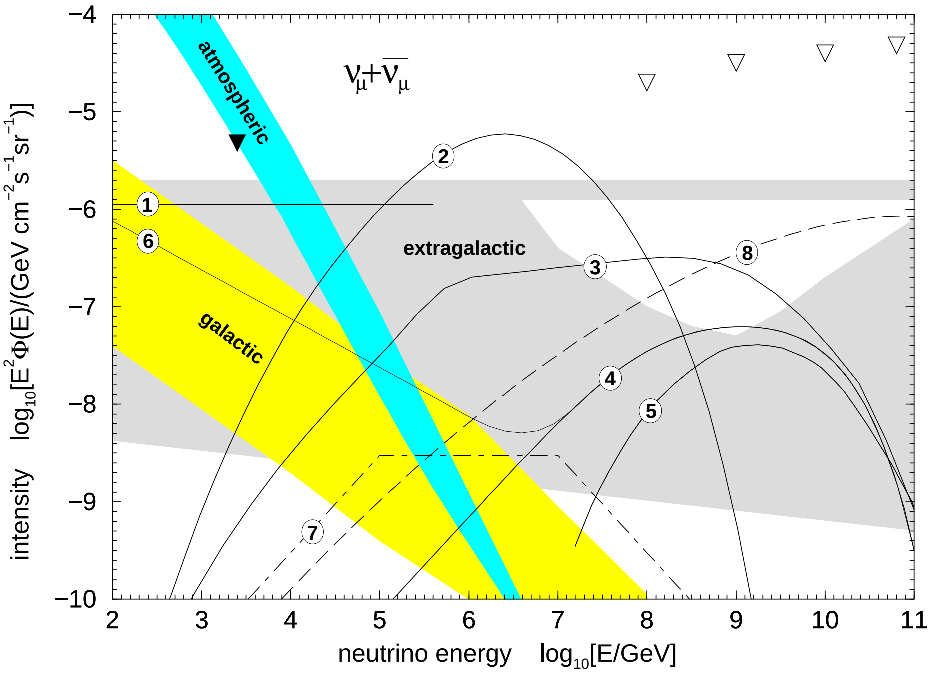

Figure 8: Summary of expected $\nu_\mu + \overline{\nu}_\mu$ intensities. Numbered lines: (1-4, 6) AGN models (Nellen 93, Stecker 96, Mannheim 95), (5) neutrinos from interaction of UHE protons with cosmic microwave background (Protheroe 96), (7) GRB model (Waxmann,Bahcall), (8) neutrinos from topological defects (Sigl 98) Shaded regions: "atmospheric": atmospheric neutrinos, in horizontal (upper boundary) and vertical (lower boundary) direction. "galactic": galactic disk toward the center (upper boundary) and the Poles (lower boundary). Shadowed background band: Theoretical bounds on diffuse fluxes from [39]. Straight upper boundary – only gamma rays escape freely from the source region. Curved upper boundary – gammas rays as well as nucleons escpae freely from the source region. Bold triangle: Frejus limit on excess above atmospheric neutrinos, blank triangle: limits on upward events from the Fly's Eye fluorescence detector. Figure taken from [33])

Models like that of Nellen et al. (1), a down-scaled version of Stecker and Salamon (2) or an up-scaled version of Mannheim (4,6) yield a few ten up to a few thousand events for IceCube.

The sensitivity of an array can be quoted in various ways. One method is to give the predicted number of events for various models. An alternative way is to assume that *no* excesses are observed and to derive the ultimate upper limit which can be obtained with the help of the given detector. We go through this excercise in the following.

The method we use has been worked out in [42]. The paper examines the problem of choosing experimental cuts in order to place the most restrictive limit on theoretical signal models in the presence of background. Although one cannot know the actual upper limit that will result from an experiment until looking to the data, one can use Monte Carlo predictions to calculate a so-called average upper limit that would be observed after hypothetical repetition of the event with a certain expected background and no true signal. This quantity is identical to the "sensitivity" defined in [47] (Feldman-Cousins limit, *FCL*). The *model rejection factor, MRF* is then defined as the ratio of the predicted signal to the Feldman-Cousins limit. Over an ensemble of identical experiments, the best *MRF* corresponds to the set of cuts which minimizes the ratio of the Feldman-Cousins limit to the signal predicted by a certain model. If the cut parameter would be the energy, as in our case, the best average upper flux limit would be defined as Flux(Energy) $\times$ *MRF*.

In the following, we use the number of hit PMTs (N_{ch}) as cut parameter. N_{ch} is highly correlated with the energy. A cut on N_{ch} is therefore at the same time a cut on the energy and can be used to separate the signal of high energy extratereestrial neutrinos from the background of atmospheric neutrinos.

4.1.1 Limit on the diffuse flux

Fig. 9 shows at top-left the differential N_{ch} distribution for atmospheric neutrinos (dashed histogram) and AGN neutrinos (full histogram). Again, a flux of $10^{-7} \cdot E^{-2}$ GeV^{-1} cm^{-2} s^{-1} sr^{-1} has been assumed for AGN neutrinos. Top right the integral N_{ch} distribution is shown. The dotted line gives the Feldman-Cousins limit. The curve at the bottom left gives the the model rejection factor *MRF* which is the ratio of the expected signal to the average upper limit as a function of N_{ch}. Finally, at bottom right the average upper flux limit is shown. At low cut values, the limit is background dominated, at higher values the signal fades away and the region is signal limited. The best cut value is given by the minimum of this curve and is in this case at $N_{ch} = 180$. It results in an upper limit of $5.5 \cdot 10^{-9} \cdot E^{-2}$ GeV^{-1} cm^{-2} s^{-1} sr^{-1}. Table 5 gives the average upper limits achievable with various IceCube configurations. Due to its background limitation, this limit scales only with sqrt(*time*). Therefore, a four-year observation would result in an improvement by a factor of two.

Table 5: Average upper limits on the diffuse AGN flux, for different configurations, in units of $10^{-9} \cdot E^{-2}$ GeV^{-1} cm^{-2} s^{-1} sr^{-1}.

vertical/horizontal	100 m	125 m	150 m	175 m
12 m	11.0	6.1	5.3	-
16 m	6.1	5.5	4.5	-
20 m	5.3	4.4	3.8	2.9

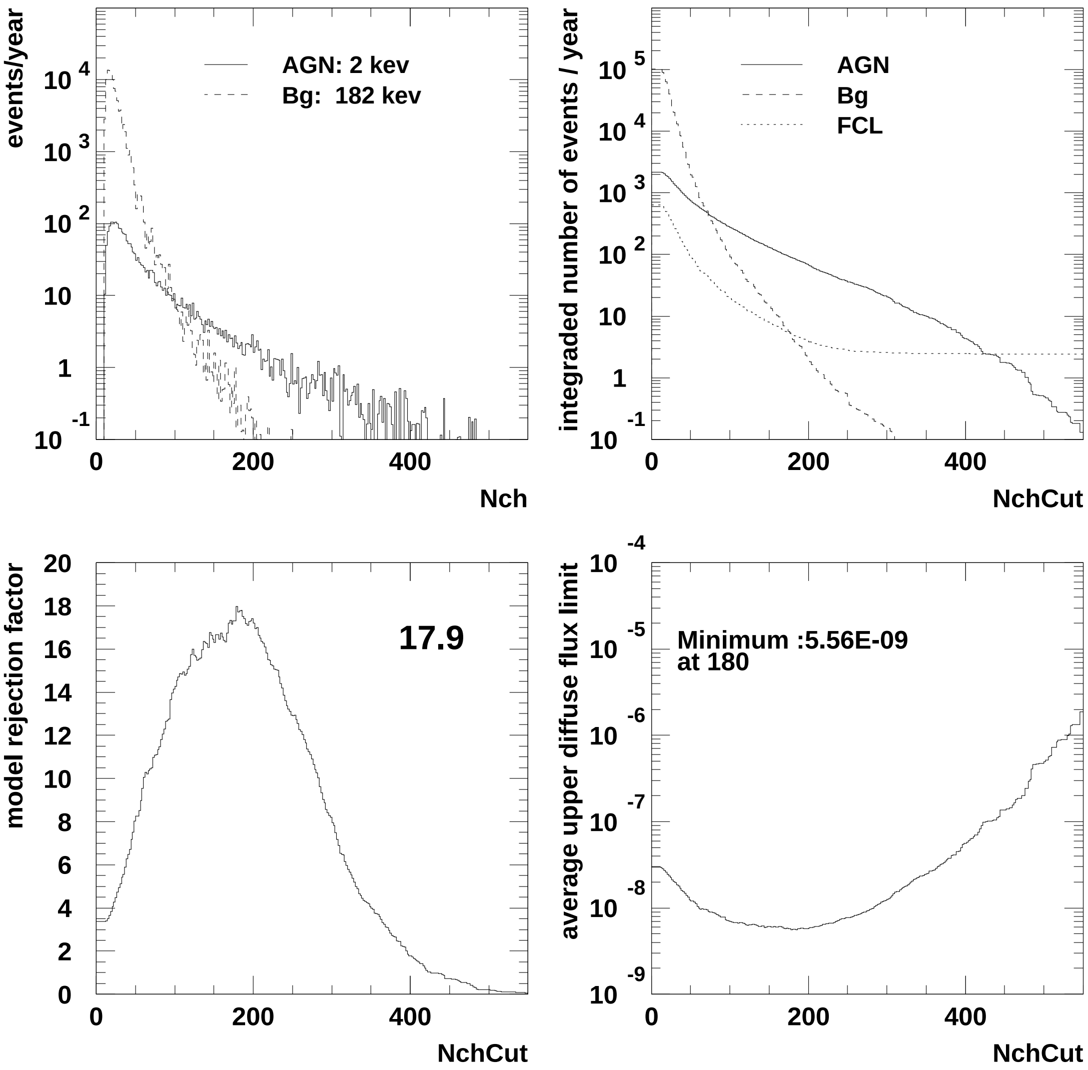

Figure 9: **Derivation of a limit on the diffuse flux:** *Top left:* differential N_{ch} distribution for atmospheric neutrinos (dashed histogram) and AGN neutrinos (full histogram), assuming a flux of $10^{-7} \cdot E^{-2}$ GeV^{-1} cm^{-2} s^{-1} sr^{-1} for AGN neutrinos. *Top right:* integral N_{ch} distribution. Dotted line – Feldman-Cousins limit. *Bottom left:* model rejection factor. *Bottom right:* average upper flux limit.

4.1.2 Limit on the flux from a point source

In the case of a point source, the background from atmospheric neutrinos is reduced by *binsize*/(1 sr). Therefore the optimum cut in N_{ch} is at a much lower value than in the case of diffuse fluxes. Figure 10 shows, at top left, the N_{ch} distribution for AGN neutrinos and atmospheric neutrinos in a $(1^o \times 1^o)$ window. Assuming an AGN flux of $10^{-7} \cdot E^{-2}$ GeV^{-1} cm^{-2} s^{-1}, one gets 142 events from AGN neutrinos and 10 events from atmospheric neutrinos. The optimum cut value for the best average limit is now at $N_{ch} = 34$ and results in a limit of $3.5 \cdot 10^{-9} \cdot E^{-2}$ GeV^{-1} cm^{-2} s^{-1}.

Table 6 gives the average limits for the different configurations. In contrast to the diffuse case, which is fully background dominated and scales like sqrt($time$), the point source limit decreases stronger with exposure time. It is $1.3 \cdot 10^{-9}$ after 4 years for 125 m string spacing, and $1.0 \cdot 10^{-9}$ for 150 m string spacing.

Also shown in figure 10 (bottom left) is the angular resolution for AGN neutrinos as a function of the N_{ch} cut. For $N_{ch} > 34$ it improves from 0.9 degrees to 0.75 degrees and asymptotically approaches 0.6 degrees.

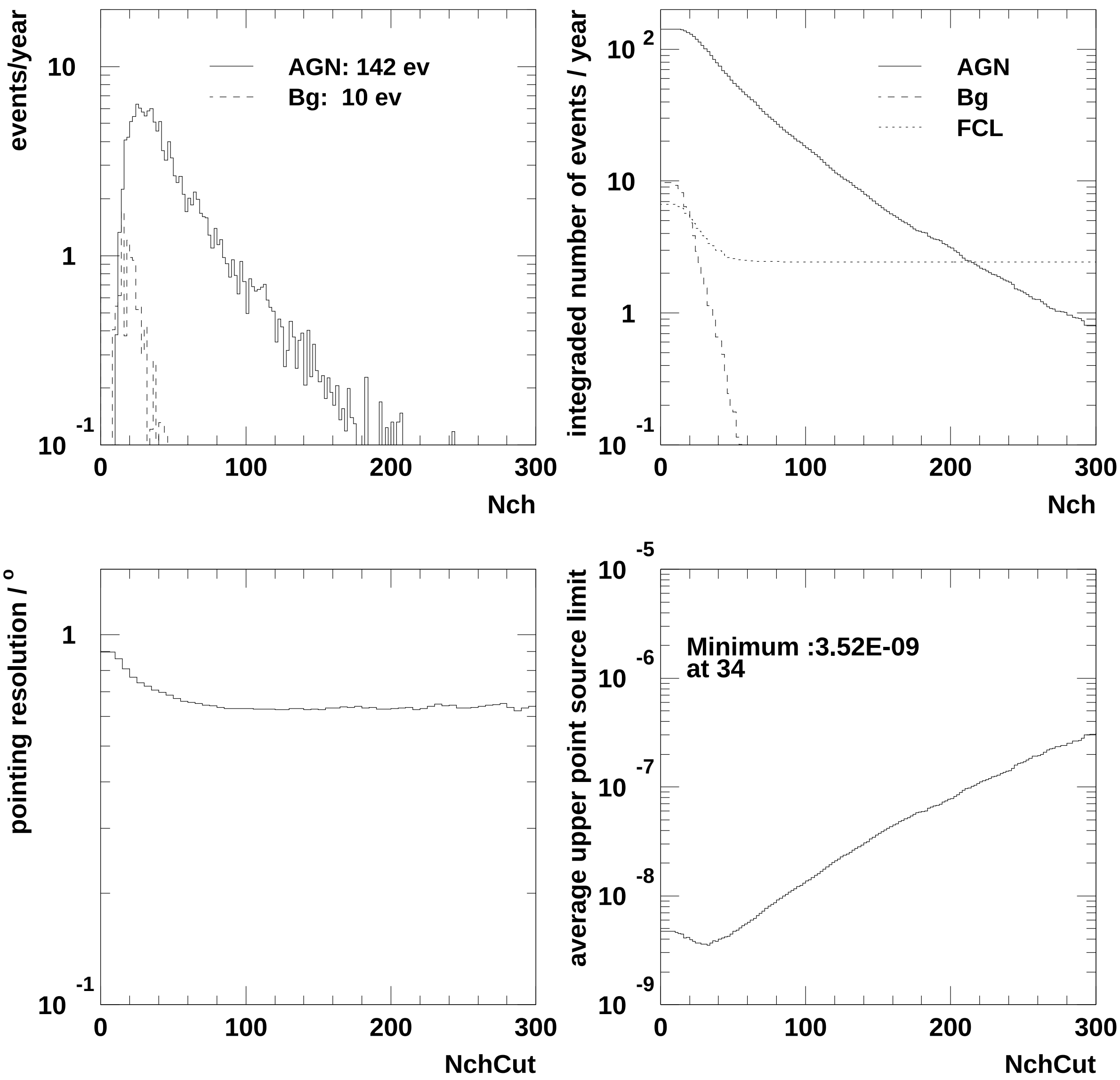

Figure 10: **Derivation of a limit on the flux from a point source** *Top left:* differential N_{ch} distribution for atmospheric neutrinos (dashed line) and AGN neutrinos (full line), assuming a flux of $10^{-7} \cdot E^{-2}$ GeV^{-1} cm^{-2} s^{-1}, for AGN neutrinos. *Top right:* integral N_{ch} distribution. Dotted line – Feldman-Cousins limit. *Bottom left:* pointing resolution as a function of the N_{ch} cut. *Bottom right:* average upper flux limit.

Table 6: Average upper limits on the flux from a point source, for different configurations and in units of $10^{-9} \cdot E^{-2}$ GeV^{-1} cm^{-2} s^{-1}.

vertical/horizontal	100 m	125 m	150 m	175 m
12 m	5.6	4.7	4.4	-
16 m	4.6	3.8	3.5	-
20 m	4.1	3.4	3.1	2.9

How does the expected IceCube limit compare to existing observations in gamma rays?

The strongest TeV gamma source on the Northern sky is the Crab, with an integral flux above 1 TeV $\sim 2 \cdot 10^{-11}$ cm^{-2} s^{-1} [43]. Fluxes of Markarian 501 vary beyween 0.5 and $10 \cdot 10^{-12}$ cm^{-2} s^{-1} for E >1.5 TeV, depending on the flaring phase [44]. Hopes for stronger sources, which might not yet have been observed by air Cherenkov telescopes since no telescope has been pointed to them, are going to be bounded by MILAGRITO [45]. They performed a full survey of the Northern sky for TeV point sources and set an upper limit of 10^{-10} cm^{-2} s^{-1} for declinations between 10 and 70 degrees and energies above one TeV.

The achievable ("average") limit of IceCube transforms to

$$F_\nu(> 1\text{TeV}) = \int_{1000}^{\infty} 10^{-9} \cdot E^{-2}\text{GeV}^{-1}\text{cm}^{-2}\text{s}^{-1} dE = 10^{-12}\text{cm}^{-2}\text{s}^{-1} \qquad (10)$$

i.e, it is nearly two orders of magnitude below the MILAGRITO limit and one order of magnitude below the observed Mk501 flux in the flaring phase.

The ratio of neutrinos to gamma rays can vary over a wide range. For a hadronic beam one expects $\nu/\gamma \sim 1$, This ratio would be valid, if all primary gammas from π^o decay would escape the source region. Actually, gammas will cascade in the surrounding medium, resulting in a flux of low-energy gammas which is much higher than that of the primary high-energy neutrinos.

If the source accelerates particles to EeV energies, one therefore would expect $\nu/\gamma \ll 1$ in the TeV range and $\nu/\gamma \gg 1$ at EeV energies. If the maximum energy of the accelerator is in the TeV-PeV range, ν/γ at TeV energies would be closer to unity. On he other hand, the ν/γ-ratio at TeV energy could be larger than unity for "cocooned" sources where gammas cascade down to keV-MeV energies before they escape.

Actually, it is just the ν/γ ratio and its dependence on energy which tells much about both the acceleration process (electron vs. hadron acceleration) and the character of the beam dump. Therefore IceCube observations with the sensitivity given above will put strong constrains on source models.

See also fig. 3 for the prediction of the signal that would be generated by a neutrino flux normalized to the level of TeV gamma emission during the extended high-state of Markarian 501 in 1997. The integral shown in the figure would give ~ 30 events per year above atmospheric background.

4.2 Possible improvements

The sensitivies given above could change in reality. We estimate that uncertainties in ice modelling might change them by up to 50% – in both directions. Use of an energy estimator better than N_{ch} may result in an improvement of up to 30%. Use of wavelength shifter could enhance the sensitivity of the OMs by up to 35% and result in correspondingly higher event numbers. The application of reconstruction methods which make use of the full waveform instead of using only the time of the first arriving photon will lead to a better angular reconstruction, in particular for high-energy events. We hope to reach an accuracy of about 0.5 degrees for moderate cuts, resulting in a slightly better point source sensitivity. Neutrinos with >100 PeV have not been taken into account in the present simulation. Their inclusion will also result in a better limit. Other lines of improvement are selection of cuts with a better passing rate for for AGN neutrinos (giving possibly a 10–15% effect), and a change of the configuration to larger spacing, which is discussed in section 6.

5 EeV Science with IceCube

A kilometer-scale neutrino observatory, though optimized for detecting neutrinos of TeV to PeV energy, can be used for EeV science and reveal the science associated with the enigmatic super-GKZ radiation in the Universe. Speculations regarding its origin include heavy relics from the early Universe, particle interactions associated with the Greisen cutoff, and topological defects which are remnant cosmic structures associated with phase transitions in grand unified gauge theories. With the capability of measuring energy, IceCube can reject the atmospheric neutrino background by identifying the very high energy of cosmic neutrino events. The instrument does not have to rely on the information that the neutrino penetrated the Earth. It therefore has sensitivity over the full solid angle, including the horizon where most of the signal is concentrated. This is critical because up-going neutrinos carrying the energies of interest here are absorbed by the Earth. Calculations in the literature have thus routinely underestimated the event rates of IceCube for EeV signals by one to two orders of magnitude by calculating only the strongly absorbed flux of up-going neutrinos.

"Ultimate" neutrino detectors of EeV energies and above [59] are contemplated reaching effective volumes of 10^{13} tons and effective areas of $10^6\,\mathrm{km}^2$ by exploiting totally novel detection methods such as radio, acoustic, atmospheric fluorescence and horizontal air shower techniques. Although much smaller and optimized for TeV–PeV rather than EeV energy neutrinos, IceCube can, because of energy measurement, do the science envisaged by future radio observatories, the Auger air shower array and the space-based atmospheric fluorescence detector OWL. Generic science includes topological defects, super-heavy relics and neutrinos produced in the interactions leading to the GKZ cutoff.

To benchmark the performance of IceCube relative to OWL [20], chosen as an example of an instrument optimized to $\sim 10^2$ EeV energy, we use the following theorized sources of super-EeV neutrinos:

- generic topological defects with grand-unified mass scale M_X of order 10^{15} GeV and a

Table 7: Comparison of neutrino event rates for three representative neutrino fluxes for OWL [20] and IceCube [18].

	Volume	Eff. Area	Threshold
OWL	10^{13} ton	10^{6} km^2	3×10^{19} eV
IceCube	10^{9} ton	1 km^2	10^{15} eV*
	Events per Year		
	TD	Z_{burst}	$p\gamma_{2.7}$
OWL ν_e	16	9	5
IceCube ν_μ	11	30	1.5

*actual threshold ~100 GeV; requiring >1 PeV eliminates atmospheric ν background.

particle decay spectrum consistent with all present observational constraints [21],

- superheavy relics [22, 23], which we normalize to the Z-burst scenario [24] where the observed cosmic rays with $\sim 10^{20}$ eV energy, and above, are locally produced by the interaction of super-energetic neutrinos with the cosmic neutrino background,
- neutrinos produced by superheavy relics which themselves decay into the highest energy cosmic rays [25], and
- the flux of neutrinos produced in the interactions of cosmic rays with the microwave background [26]. This flux, which originally inspired the concept of a kilometer-scale neutrino detector, is mostly shown for comparison.

In Table 7 we compare the event rates for IceCube with those for OWL calculated in [20]. The conclusion is clear, while effective volume and area for OWL apparently exceed those of IceCube by many orders of magnitude, the events rates are comparable. This is a consequence of the duty cycle, reduced efficiency, and higher threshold of the OWL detector. Note that the primary mission of OWL is cosmic ray, not neutrino physics. An equally valid conclusion is that OWL can reach similar event rates to a dedicated neutrino detector.

One notices that the event rates claimed for IceCube are roughly two orders of magnitude larger than those found in the literature for a generic detector with 1 km^2 effective area. The reason for this is simple. Although this is not the case for first-generation neutrino telescopes, we here assumed that IceCube can measure energy, and can, therefore, separate interesting high energy events from the background of lower energy atmospheric neutrinos by energy measurement. Thus the instrument can identify high energy neutrinos over 3π or even 4π solid angle, and not just in the lower hemisphere where they are identified by their penetration of the Earth, as is the case with AMANDA. This is of primary importance here because neutrinos produced, for instance by the decay of topological defects, have energies large enough to be efficiently absorbed by the Earth. The observed events are dominated by neutrinos interacting in the ice or atmosphere *above* the detector and near the horizon where the atmosphere alone represent a target density for converting neutrinos of 36 kg/cm^2. This event rate typically dominates the one for up-going neutrinos by an order of magnitude. The zenith angle distribution of neutrinos associated with EeV signals forms a striking signature for their extremely high energy origin.

6 On the possible modification of late IceCube stages towards higher energies

The default IceCube configuration is optimized for the energy region of 1-100 TeV, with a reasonable (i.e. economic) performance up to several PeV. For higher energies, the 125 m string spacing is going to be less economic, and a larger spacing would preferable: still, all muons crossing the array would be detectable (i.e. there would be no "blind" corridors), but the geometrical area would be larger.

Lets consider a scenario with no positive observations after four years AMANDA-II observations and additionally 2 years observations with the first 6+12=18 IceCube strings, corresponding to 150 000 to 200 000 m$^2 \times$ year. This would push the limit on diffuse fluxes down to a level, where the limit is purely background determined – see figure 11 – with the background being atmospheric neutrinos. That means that with respect to the energy range for which IceCube is optimized, the diffuse limit would improve only like $sqrt$(observation time). Therefore, the most economic use of new strings would be to deploy them with an increased spacing, corresponding to higher muon energies.

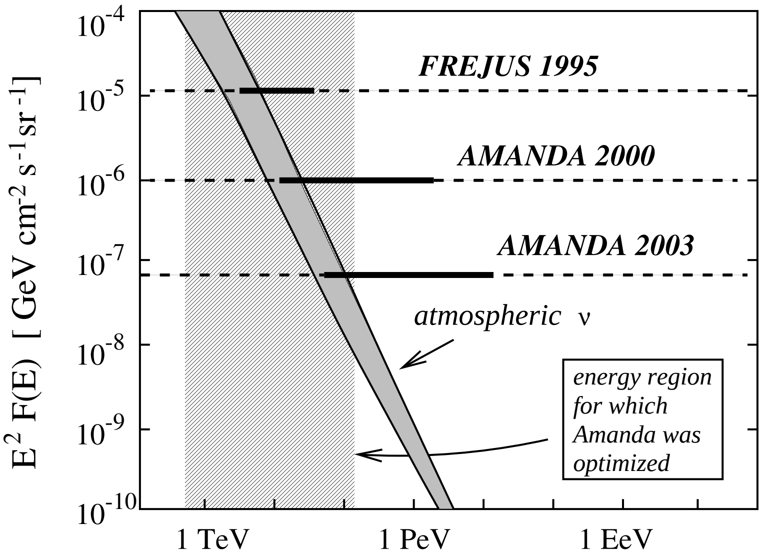

Figure 11: Sensitiviy for diffuse AGN fluxes obtained at present and expected for the future with Amanda, shown with the background from atmopsheric neutrinos and confronted with the energy range for which present underwater projects are optimized.

Another argument in favor of larger spacing was made in [48]. Assume that the limit at

TeV energies is pushed below the level of atmospheric neutrinos and the search for excesses is focussed to the PeV-EeV region. At these energies the Earth is opaque for neutrinos (see figure 5, and signals can be expected only from the side or from above. Figure 12 sketches the ranges of zenith angle typical for the various energies. The background of background events due to downward muons from air showers above the array becomes smaller with increasing energy. Actually it is expected so small that at EeV energies the search region can be extended much above the horizon, to zenith angles of 40-60 degrees or even less [49].

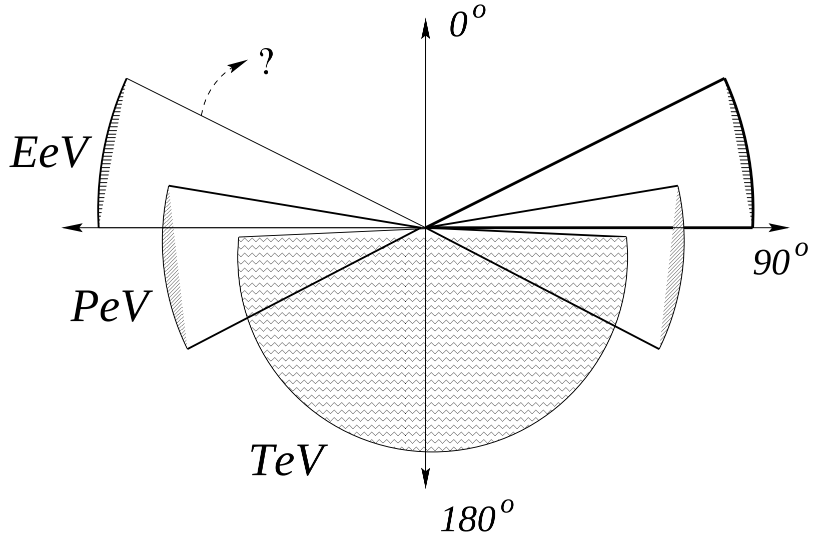

Figure 12: Typical zenith angle ranges for various energies regimes.

If the signal comes preferentially from the side, a further upgrade of the detector with unchanged string spacing and the same string length would mean that the effective area increases only with sqrt($N_{strings}$).[2] For PeV-EeV physics, one therefore would make a considerably more economical use of further strings, if one increases their spacing.

The consequences of background limitation given above apply to diffuse fluxes. For steady point sources, and the more for transient sources, the background is small or negligible and the sensitivity of IceCube would improve stronger than with the square root of time or the number of strings. Table 8 summarizes, for various physics goals, the behavior of the sensitivity as a function of observation time and of the number strings with fixed spacing.

We note again that in the case of very high-energies the square root behavior can be made more linear by larger string spacing.

After the arguments outlined above the question arises, why not the IceCube spacing should be chosen large from the very beginning. The answer is simple: A large spacing would deteriorate the low-energy capabilities of the array (at $<$ a few TeV). An E^{-2} behavior is

[2]Imagine a detector with 0.5 km $\times$ 0.5 km seen from the top (5×5 strings), and a string length of 1 km. Its area seen from the side is 0.5 km^2. If now the side length is increased by a factor two, the detector seen from top would have dimensions 1.0 km $\times$ 1.0 km, and the number of strings would have increased by a factor of four. Seen from the side, the geometrical area would be 1 km^2. That means that multiplying the number of strings by four would increase the area by a factor of two only - i.e. increase with sqrt($N_{strings}$). Note that this argument is valid only if the spacing remains unchanged!

a simplification, and actually most of the models predict a different energy dependence (see figure 5). Several models published recently even predict maximum neutrino fluxes in the TeV range. As examples, we mention the AGN model [52] which predicts flares of 100 GeV - few TeV neutrinos lasting over several days or even weeks, various GRB models which predict neutrino bursts at >5 TeV [50], or with two bumps - the one at 10 GeV, the other at 100 TeV [51], and recent preditions for TeV-neutrinos associated with supernova bursts [53].

Figure 13 shows a 10-TeV track in IceCube, figure 14 a 6-PeV muon track. One indeed notices that for these high energies the default IceCube configuration might turn out to be overequipped and a larger spacing could be considered.

Table 8: Scaling of the sensitivity with data taking time and number of strings for various goals and an detector of IceCube size

physics goal	scaling with observation time	scaling with number of strings	remarks
transient sources like GRB	linear	linear	
point sources			
$\leq$ 100 TeV	linear	linear	
100 TeV - 10 PeV	linear $\rightarrow$ sqrt	linear $\rightarrow$ sqrt	
> 10 PeV	sqrt	sqrt	
diffuse flux			
< 1 PeV	sqrt	linear	
1 -10 PeV	sqrt$\rightarrow$ linear	linear $\rightarrow$ sqrt	
EeV	linear	sqrt	
WIMPs in Earth	sqrt	sqrt	background from atm. ν
WIMPs in Sun	sqrt	linear $\rightarrow$ sqrt	background from CR interaction in the Sun
monopoles	linear	linear	
Supernova	-	sqrt(N_{OM})	limited by PMT dark-noise
cascades			
< 10 TeV	sqrt	stronger than linear	limited by brems - cascades
> 1 PeV	sqrt/linear	stronger than linear	strong increase with N_{string} due to better containment

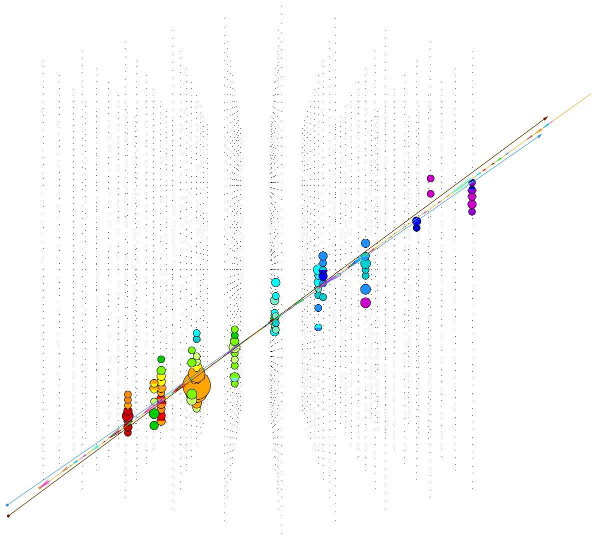

Figure 13: A 10-TeV muon track in IceCube.

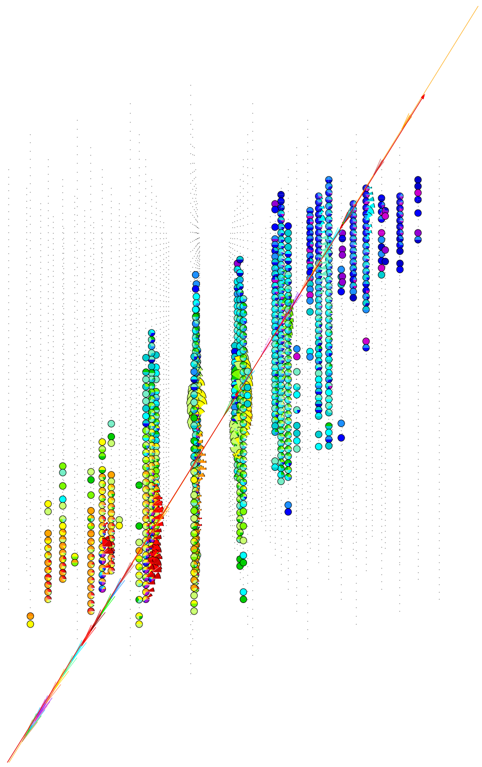

Figure 14: A 6-PeV muon track in IceCube.

7 Detection of Tau Neutrinos in IceCube

7.1 Tau Neutrino Detection

High energy tau neutrinos can be detected using the characteristic double bang events in which the production and decay of a τ lepton can be identified [27]. In a charged current ν_τ deep inelasticscattering (DIS) interaction with a nucleus, a τ lepton of energy $(1-y)E_{\nu_\tau}$ is produced as well as a hadronic shower of energy yE_{ν_τ} which is initiated in the fragmentation of the nucleus. Here y is the fraction of energy transferred to the hadronic vertex in the interaction. The tau lepton travels on average a distance R_τ along the medium before decaying given by:

$$R_\tau = \frac{E_\tau}{m_\tau} ct_0 = \frac{(1-y)E_{\nu_\tau}}{m_\tau} ct_0 \tag{11}$$

where E_τ and m_τ are the energy and mass of the τ respectively and t_0 is its rest lifetime. The τ is not expected to have high energy losses before decaying. In its decay it produces another ν_τ and an electromagnetic or hadronic shower $\sim$ 82% of the times. Assuming a typical detector dimension D, there are several conditions that have to be fulfiled for the detection of a double bang event inducedby a ν_τ:

- The ν_τ has to interact through a charged current DIS interaction producing a hadronic shower contained inside the instrumented volume of the detector ($\sim D^3$).
- The τ lepton must decay inside the detector through a channel that produces an electromagnetic or hadronic shower which again has to be contained inside the neutrino telescope.
- R_τ has to be large enough so that both showers are sufficiently separated from each other to be distinguished.

Figure 15 shows a simulated CC ν_τ event in IceCube.

We have calculated the probability of detecting a double bang event in a neutrino telescope of linear dimension $D = 1$ km such as IceCube. We have developed a very simple Monte Carlo for this purpose in which the detector is considered as one dimensional. We have taken the energy threshold for detecting showers to be $E_{\text{shower}} \sim 1$ TeV. We have fixed to 250 m the minimum distance the τ has to travel to clearly distinguish the Cherenkov light from both showers. This number is mainly determined by the separation between PMT's which is 125,m. Our Monte Carlo accounts for the fluctuations in the fraction of energy transferred to the τ in the interaction, as well as for the fluctuations in its range. The result of the Monte Carlo is shown in Fig.16 along with the probability of observing a ν_μ-induced muon. Also shown is the probability of observing a double bang event as obtained in [28] using the expression:

$$P_\tau(E, E_\tau^{\min}) = \rho N_A \int^{1-\frac{E_\tau^{\min}}{E}} dy [D - R_\tau] \frac{d\sigma^{CC}(E,y)}{dy}, \tag{12}$$

where ρ is the density of the medium and N_A is Avogadro's number. $E_\tau^{\min}$ is the minimum energy of the τ, it is automatically fixed imposing that $R_\tau \geq 250$ m. This expression uses

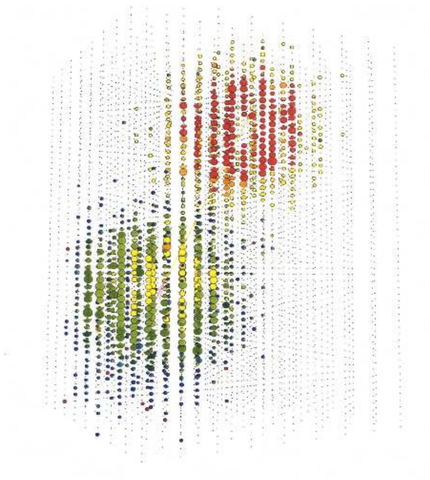

Figure 15: A double-bang ν_τ event with an energy of a few PeV in IceCube

average values for R_τ and hence at $E_{\nu_\tau} \le E_\tau^{\rm min}$ the probability of observing a double bang vanishes since the average range of the τ is smaller than 250 m. The probability calculated with this expression has a broad maximum which is determined by the condition that R_τ has to be larger than250 m but smaller than the size of the detector. Assuming an average value of $y \sim 0.25$ at these energies and using expression (11) this corresponds to E_{ν_τ} between roughly 7 PeV and 27 PeV.

Due to fluctuations in R_τ, even ν_τ's with energy below $E_\tau^{\rm min}$ are going to produce τ's that travel more than 250 m. This explains why our probability doesn't vanish at $E_{\nu_\tau} < E_\tau^{\rm min}$ as happens to the one given by Eq. (12). It also has a longer tail at high energies because fluctuations in the τ range and in its energy prevent a fraction of high energy ν_τ's from producing a τ that travels a distance larger than the dimension of the detector.

7.2 Neutrino Event Rates

We calculate the number of ν_τ events in the standard way [12], convoluting the probability of observing the double bang events with the $\nu_\tau + \bar{\nu}_\tau$ flux:

$$N_{\rm events} = A_{\rm eff} \int \Phi_{\nu_\tau + \bar{\nu}_\tau}(E_{\nu_\tau}) P_{\nu_\tau \to \text{ double bang}}(E_{\nu_\tau}) dE_{\nu_\tau} \tag{13}$$

where we will take $A_{\rm eff} = 1$ km^2. $P_{\nu_\tau \to \text{ double bang}}$ is the probability of observing a double bang event as shown in Fig.2.

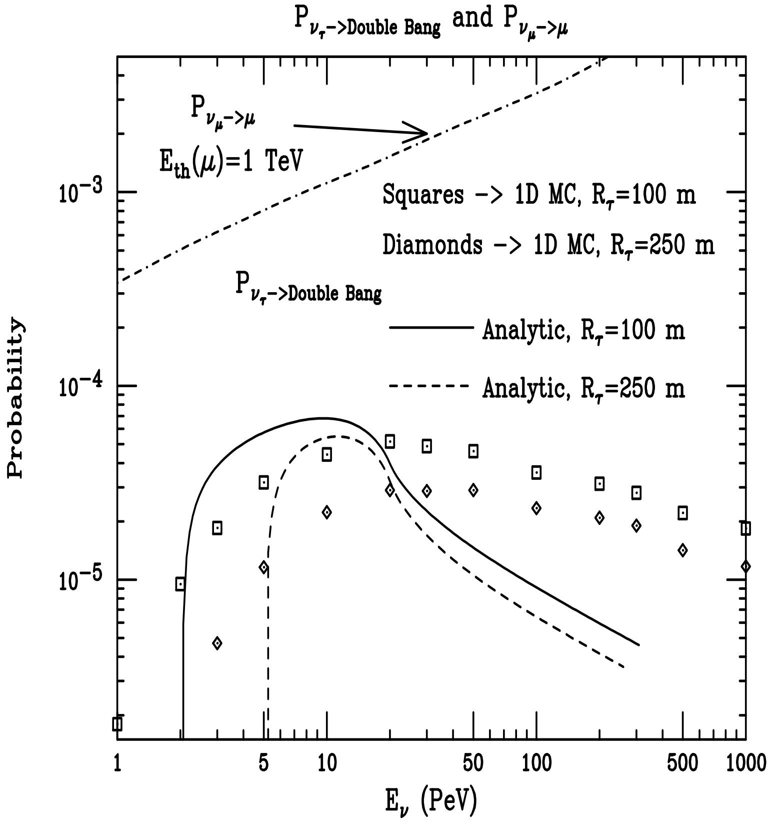

Figure 16: Probability of detecting ν_τ induced double bang events in IceCube obtained with Monte Carlo simulation and using the analytic expression given by of [28] (Eq.2). The probability is shown for $R_\tau = 100\,\mathrm{m}$ and $250\,\mathrm{m}$. Also shown is the probability of detecting a ν_μ-induced muon.

By far the largest uncertainty in this expression is the $\nu_\tau + \bar{\nu}_\tau$ flux. ν_τ production is expected to be very small in most astrophysical scenarios where ν's are produced in pp or pγ collisions. Several calculations suggest a ratio [28] $F_{\nu_\tau/\nu_\mu} \sim 10^{-5}$

Oscillation scenarios in which ν_μ's convert themselves into ν_τ's may be the most promising sources of ν_τ's. In fact the detection of ν_τ events in numbers which are not compatible with the expected astrophysical production, may be indicative of such oscillations. In any case the non-observation of events may place limits on several oscillation scenarios. Making the rough assumption that $F_{\nu_\tau/\nu_\mu} = 0.5$ we obtain the number of events in Table 9 for representative $\nu_\mu + \bar{\nu}_\mu$ fluxes in the literature. In Fig.3 we also show the energy distribution of the events. They all ressemble the shape of the probability function of Fig.2.

For more details and references, see J. Alvarez et al. [2].

Table 9: Double bang events per km^2 per year in 2π stereoradian for representative $\nu_\mu + \bar{\nu}_\mu$ fluxes in the literature assuming $F_{\nu_\tau/\nu_\mu} = 0.5$. Attenuation has been taken into account to calculate ν_μ events but not for ν_τ events. The GRB event rate takes into account fluctuations in distance, gamma factor and energy of the GRB's normalizing to 1000 GRB's/year. The TD's models correspond to maximal predictions of fig.2 in reference [21]. The neutrino flux from the decay of Superheavy Relics is taken from reference [22].

Flux	Double Bang events	$\nu_\mu + \bar{\nu}_\mu$ (upgoing) events
$10^{-6}\ E^{-2}(\text{cm}^2\ \text{s sr})^{-1}$	6	10,779
GRB (Fluctuation model)	~ 1	43
TD, $M_X = 10^{14}$ GeV, $Q_0 = 6.31 \times 10^{-35}$, p=0	146	58,665
TD, $M_X = 10^{14}$ GeV, $Q_0 = 6.31 \times 10^{-35}$, p=1	6×10^{-2}	12
TD, $M_X = 10^{14}$ GeV, $Q_0 = 6.31 \times 10^{-35}$, p=2	1.5×10^{-2}	3
TD, $M_X = 10^{15}$ GeV, $Q_0 = 1.77 \times 10^{-34}$, p=0	120	48,605
TD, $M_X = 10^{15}$ GeV, $Q_0 = 1.58 \times 10^{-34}$, p=1	5.5×10^{-2}	9
TD, $M_X = 10^{15}$ GeV, $Q_0 = 1.12 \times 10^{-34}$, p=2	1.1×10^{-2}	2
Superheavy Relics $M_X = 10^{14}$ GeV	3×10^{-2}	4×10^{-4}

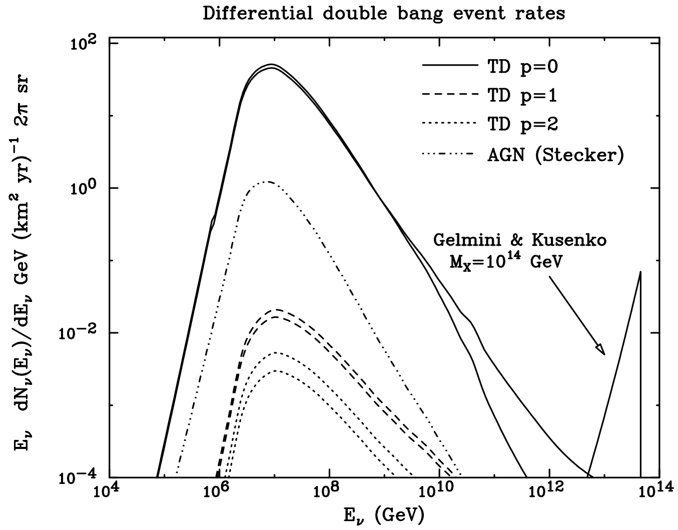

Figure 17: Differential ν_τ induced double bang event rates for different fluxes assuming $F_{\nu_\tau/\nu_\mu} = 0.5$. The upper lines at 10^7 GeV for the Topological Defect models correspond to $M_X = 10^{14}$ GeV and the lower ones to $M_X = 10^{15}$ GeV.

8 Other science goals

8.1 Relativistic magnetic monopoles

Several theories predict the existence of magnetic monopoles with a magnetic charge which obeys the Dirac quantization rule $g = n \cdot e/(2\alpha)$ with $n = 1, 2, 3, ...$ and $\alpha = 1/137$. A magnetic monopole with unit magnetic Dirac charge $g = 137/2 \cdot e$ and a velocity β close to 1 would emit Cherenkov radiation along its path, exceeding that of a bare relativistic muon by a factor of 8300 for $\beta = 1$. The value 8300 is obtained from $(137/2)^2$ multiplied with n_r^2, with $n_r = 1.33$ being the refractive index of water. This is a rather unique signature. Figure 18 shows the light emission from a monopole as a function of β. Note that due to the production of δ electrons, the monopole produces light even below its own Cherenkov threshold.

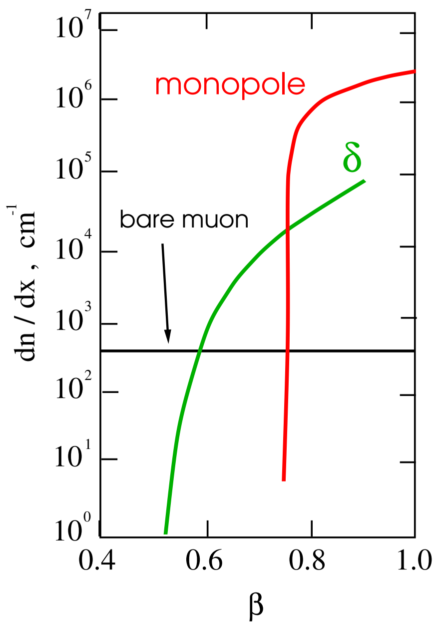

Figure 18: Cherenkov light emission from magnetic monopoles in water (in photons per cm) as a function of velocity.

Any early Universe phase transition occuring after inflation has the potential to populate the Universe with a flux of magnetic monopoles. Observations of galactic magnetic fields, as well as observations matched with models for extragalactical field lead to the conlcusion that monopoles of masses below 10^{15} GeV can be accelerated in these fields to relativistic velocities [54]. Figure 19 summarizes the limits obtained until now. Note that these limits are below the so-called Parker bound ($10^{15}\,\mathrm{cm}^{-2}\,\mathrm{s}^{-1}\,\mathrm{sr}^{-1}$). This bound is is derived from the very existence of galactic magnetic fields which would be destroyed by a too high flux of magnetic monopoles.

A cube kilometer detector could improve the sensitivity of this search by about two orders of magnitude compared to the present Amanda limit. As mentioned above, the search could be extended to down to velocities $\beta \sim 0.5$ by detecting the δ electrons generated along the monopole path.

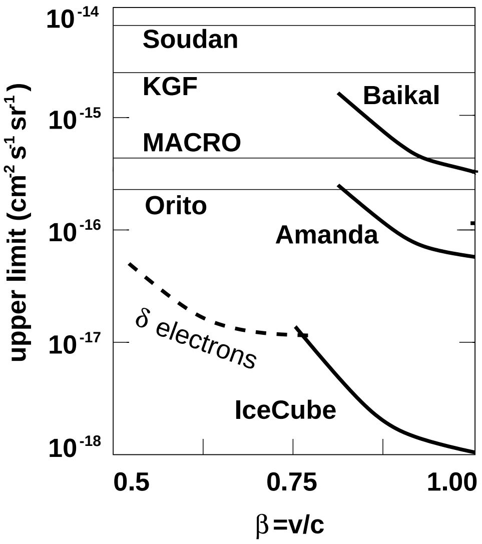

Figure 19: Present limits on the flux of relativistic monopoles compared to limits achievable with IceCube.

8.2 Slowly moving, bright particles

The passage of a particle with a velocity significantly below c yields a very distinct time pattern.

Candidates for particles with a velocity $\beta < 0.1\,c$ and with strong light emission are GUT magnetic monopoles or nuclearities [29, 55]. GUT monopoles may induce protons decays. Therefore one would expect Cherenkov light signals generated by the nucleon decay products along the path of the monopoles. For certain regions of the parameter space in monopole velocity and catalysis cross section, these signals would cause sequential hits in individual PMTs within time windows of $10^{-5} - 10^{-3}$ s.

Nuclearities (strange quark matter) should be aggregates of u, d and s quarks in equal proportions, and of electrons, to ensure their electrical neutrality. They should be stable for all baryon numbers in the range between ordinary nuclei and neutron stars ($A \sim 10^{57}$). They could have been produced in the primordial Universe or in violent astrophysical processes. See for recent reviews [55, 56].

The most relevant upper limits on the flux of these particles come from track etch experiments or liquid scintillator experiments (both e.g. represented by MACRO). The Baikal experiment has searched for enhanced counting rates over time intervals of 500 μs and deduced upper limits on the flux of GUT monopoles and strange quark matter [29]. The search technique relies on detectors with a low counting rate. In the Baikal case a rate as low as 100 Hz is achieved by local coincidences. With a counting rate per OM of 300 Hz (compared to typically 1 kHz for AMANDA), also IceCube may look for corresponding phenomena.

8.3 Neutrinos from WIMP annihilation

If Weakly Interacting Massive Particles (WIMPs) make up the dark matter of the universe, they would also populate the galactic halo of our own Galaxy. They would get captured by the Earth or the Sun where they would annihilate pairwise, producing high-energy muon neutrinos that can be searched for by neutrino telescopes. A favorite WIMP candidate is the lightest neutralino which arises in the Minimal Supersymmetric Model (MSSM).

The typical energy of the neutrino-induced muons would be of the order of $\leq 25\%$ of the neutralino mass. Since the muon threshold for IceCube is expected to be fairly high ($\sim 100\,\mathrm{GeV}$), we expect IceCube to be sensitive mainly to neutralinos heavier than about 400 GeV.

In [30] the performance of IceCube was studied for two configurations, a 9 string $\times$ 9 string pattern with 125 m string spacing and a detector consisting of eight sub-modules of 10 strings each, with string spacing of $70 - 90\,\mathrm{m}$ within the sub-detectors (see figure 20).

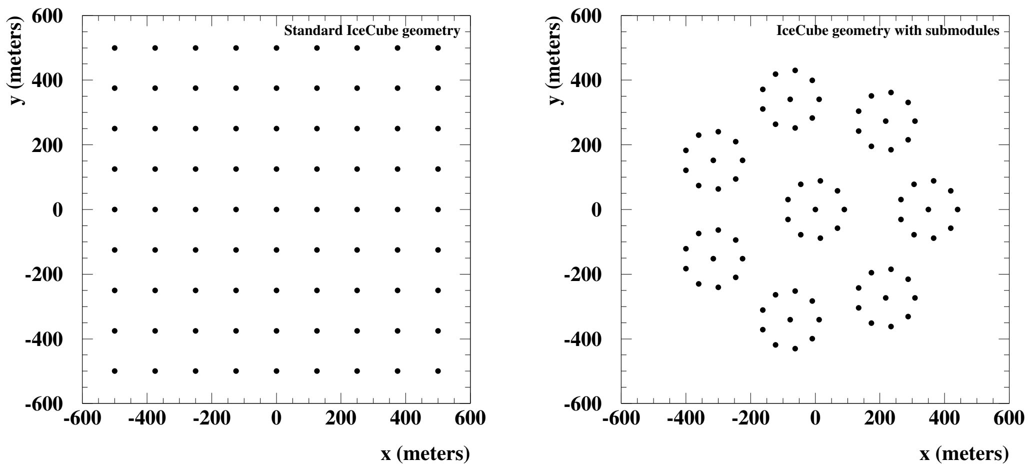

Figure 20: Configurations studied in [30]

The effective area for WIMP detection depends on the WIMP mass as well as on the typical decay channel ("soft" channels from WIMP decays into many secondaries, "hard" channels from decays into a few secondaries only). Figure 21 shows effective volumes and effective areas for the rectangular pattern ("standard" geometry, left) and the modular pattern (right), separately for neutrinos from the Sun and the center of the Earth, and for soft and hard spectra, respectively. The standard geometry gives about 0.7 square kilometer area for both solar and terrestrial WIMPs, provided the decay channels are preferentially hard. For soft channels, the area drops down to less than 200 000 m^2 for WIMP masses of 200 GeV. Compared to the standard geometry, the modular geometry gives somewhat worse results for hard decay channels and slightly better results for soft channels.

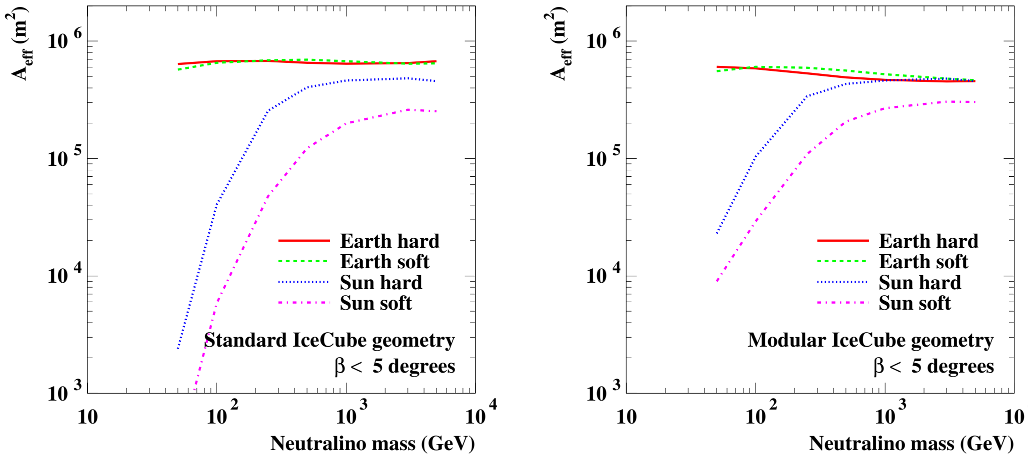

Figure 21: Effective area after a 10-degree cut on the angle between the reconstructed muon and the angle of the source, for different annihilation places, annihilation channels and WIMP masses. Results for the standard geometry to the left and for the modular geometry to the right.

Figure 22 shows the predicted muon rates from WIMPs annihilating in the Earth and the Sun as a function of the WIMP mass. Shown are results for the standard configuration with simple quality cuts after reconstruction. Each symbol in the plot corresponds to one particular combination of MSSM parameters (with the WIMP mass being one of them). Lines indicate the limits which could be achieved with IceCube after 5 years observation. Different symbols mark MSSM versions which are currently ruled out by direct detection experiments, which could be seen by direct detection experiments if the sensitivity is increased by a factor of ten, and which could not be seen by present direct detection experiments even after tenfold increase in sensitivity, respectively. All values are normalized to 10 GeV threshold for reasons of comparison[3]. It has been shown in [30] that IceCube could play a complementary role to future direct detection experiments (like CRESST or GENIUS) for annihilation in the Earth, and even has a slight advantage over direct detection experiments for certain low-mass WIMP models and annihilation in the Sun.

Figure shows the present AMANDA limit after 132 days observation time in comparison with the limits obtained from long-year exposure of MACRO, Baksan and Super-K [32]. Note that the Amanda limit is determined by our until now large systematic uncertainties which have been corrected for (the other experiments did not include their – comparatively small – uncertainties)

[3]For certain directions the IceCube energy threshold indeed might be reduced below 20 GeV. If the track of the secondary muon is close to the vertical and close to an individual string (say less than ~7 m), PMT amplitudes will be high, scattering effects will be small, and consequently arrival time jitters will be small. Under these conditions not only the muon energy can be determined with an accuracy of a few GeV from its track length, but also the vertex cascade may be identified and its energy determined. Taken all strings together, one obtains a detection volume of 10 Megatons at a threshold of 20 GeV.

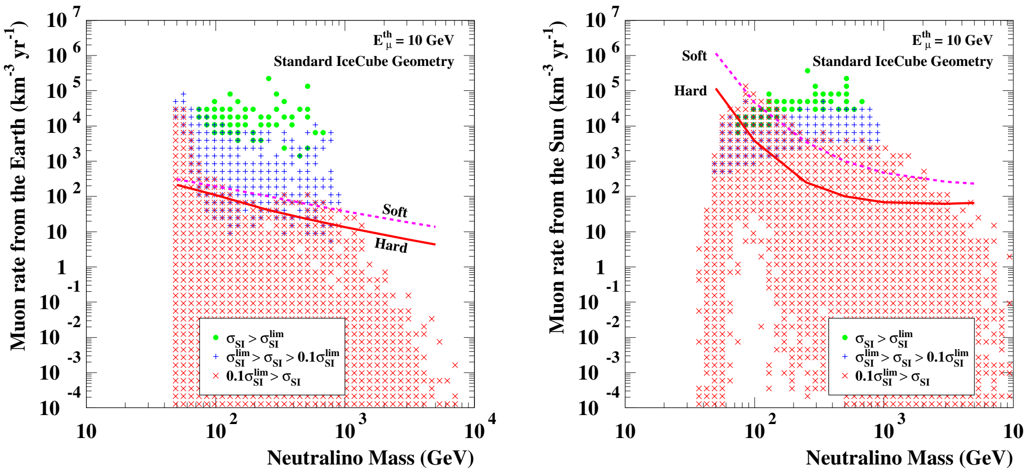

Figure 22: The predicted muon rates from WIMPs annihilating in the Earth (left) and the Sun (right) as a function of the WIMP mass. Each symbol in the plot corresponds to one particular combination of MSSM parameters. Lines indicate the limits which could be achieved with IceCube after 5 years observation. Different symbols mark MSSM versions which are currently ruled out by direct detection experiments (dots), which can be seen by direct detection experiments if the sensitivity is increased by a factor of ten (+), and which could not be seen by present direct detection experiments even after tenfold increase in sensitivity ($\times$), respectively.

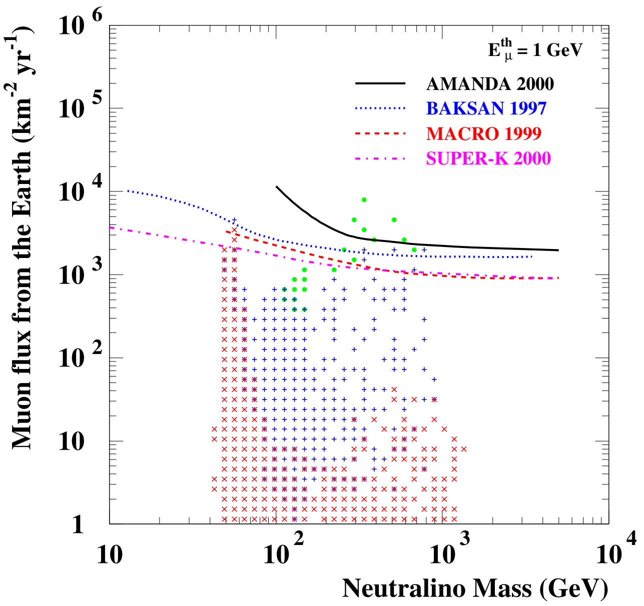

Figure 23: Upper limits on the flux of upgoing muons from WIMP annihilation in the Earth obtained in Amanda, Macro, Baksan and Super-K (normalized to 1 GeV threshold).

8.4 Neutrino oscillations

With a 10 Megaton detector of 20 GeV threshold, IceCube may also play a role in confirming the compelling indications that atmospheric neutrinos oscillate. Studies of systematics and backgrounds have revealed that significant progress requires much smaller spacing of OMs along a string than presently planned (namely 4-6 meters). For reduction of the threshold toward the horizon also a considerably smaller string spacing would be necessary. Such specialized effort is only warranted if ongoing experiments fail to conclusively prove the oscillation hypothesis. In that case one would consider to create a densely equipped region for detection of low-energy contained events as one part of IceCube. This region would be nested in the full array which acts as veto against through-going tracks. A possible solution would be to fill AMANDA-II with additional strings with small OM spacing. Note that interpretation of the feeble angular dependent oscillation effects at high neutrino energies require an extremely good understanding of the detector systematics.

In recent papers [31], the possibility is discussed to direct a neutrino beam to IceCube - either a WBB beam or a beam from a neutrino factory. The short duty time of an accelerator would allow to relax the cuts for background suppression since during the short spill times the detector is nearly free of background. The aim would be to measure mixing angle θ_{13} and the sign of Δm^2_{31}, even though it is not possible to discriminate between charges. However, it has has to be investigated how well dicrimination between muon tracks and ccascades at low energies would work.

8.5 MeV neutrinos from Supernovae

Most of the energy released by a supernova is liberated in a burst lasting about ten seconds. Roughly equal energies are carried by each neutrino species with a thermal spectrum of temperature 2–4 MeV. Since the $\bar{\nu}_e$ cross-section on protons in the detector is significantly larger than the interaction cross sections for the other neutrino flavors, $\bar{\nu}_e$ events dominate the signal by a large factor after detection efficiency is taken into account. In this reaction, free protons absorb the antineutrino to produce a neutron and a positron which is approximately isotropically emitted with an energy close to that of the initial neutrino. A thermal spectrum of temperature 4 MeV, when folded with an inverse beta decay cross section which increases with the square of the neutrino energy, yields an observed positron energy distribution which peaks in the vicinity of 20 MeV. The track-length of a 20 MeV positron in ice is roughly 12 centimeters and therefore over 3000 Cherenkov photons are produced.

Although these energies are far below the Amanda/IceCube trigger threshold, a supernova could show up by higher counting rates of individual PMTs over a time window of 5-10 s. The enhancement in rate of *one* PMT will be buried in dark noise signals of that PMT. However, summing the signals from *all* PMTs over 10 s, significant excesses can be observed. It is one of the greatest assets of Amanda, with its background rate more than 10 times lower than in Ocean experiments, that it has the potential to see a supernova and to generate an alarm signal.

Figure 24 shows, for 215 days of live time in 1997/98 and all stable Amanda-B10 PMTs , the distribution of the deviation $\Delta\mu$ of the average noise rate from its mean value. Each data point is the average over a 10-sec interval. Accepting every 10-sec interval with $\Delta\mu > 4\,\text{Hz}$ (see the vertical line) as a supernova event, would result in one fake alarm per year. This corresponds to a 90% efficiency for a SN-1987A-like supernova event loacted at a distance of 9.8 kpc (the distance to center of Galaxy is about 8 kpc). A robust on-line monitor would be operated with a slightly higher threshold covering about 70% of the Galaxy.

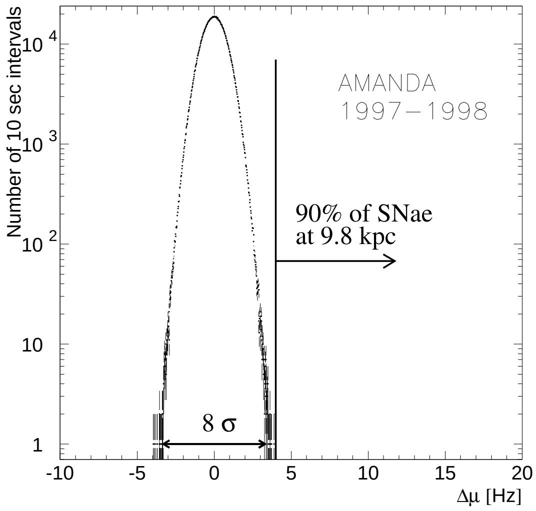

Figure 24: Distribution of the deviation $\Delta\mu$ of the average noise rate from its mean value, for 215 days of live time. The vertical line is set at the level where we get a rate of one background event per year. 90% of the supernova neutrino bursts located at 9.8 kpc distance would be seen above that cut.

With Amanda-II and an improved supression of non-poissonian noise we monitor more than 90% of the Galaxy. IceCube, with low-potassium glass spheres[4], might barely reach the the Large Magellanic Cloud.

Amanda is officially, and will be factically in the near future, a member of the Supernova Early Warning System (SNEWS) [61]. The role of Amanda will be to yield one of several coincident alarm signals from different detectors like Super-K, LVD and SNO (Macro being shut down in the mean time). On top of that, IceCube might participate in the goal to estimate the supernova direction by triangulation [60].

Figure 25 shows the increase in counting rate as seen in Amanda-II and IceCube. Given a known template for time evolution of the pulse, the resulting accuracy in timing could be 14 ms for Amanda-II and as good as 1-3 ms for IceCube. The resulting angular resolution depends on the orientation of the triangulation grid with respect to the supernova. For the three detectors Super-K, SNO and IceCube it would between typical values of 5 to 20 degrees. Figure 26 shows the χ^2-contors of reconstructed supernova direction for a randomly choosen supernova event.

With dedicated detectors like Super-K, one can determine the neutrino direction from electron direction measurement in $\nu\, e^-$ interaction with an accuracy of about 5^o.

[4]K-40 decays in the glass sphere are the main source of external noise.

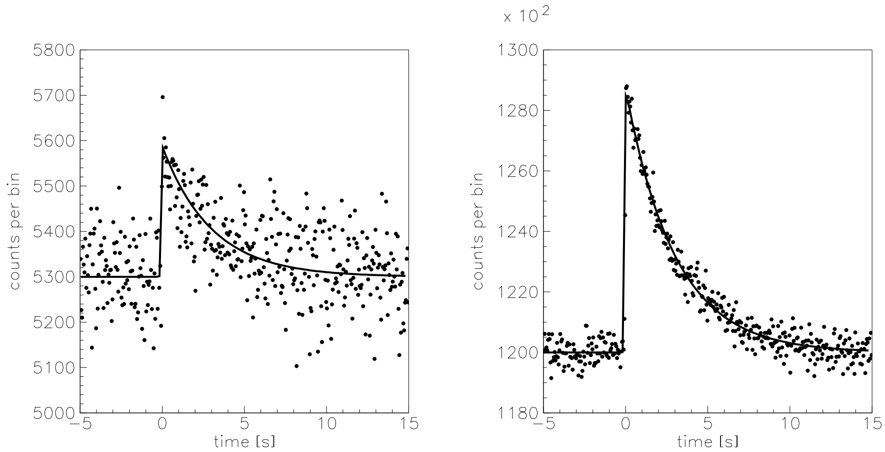

Figure 25: Simulated count rate data for a supernova at the center of the Galaxy, for AMANDA-II (left) and IceCube (right). The lines correspond to the simulation input.

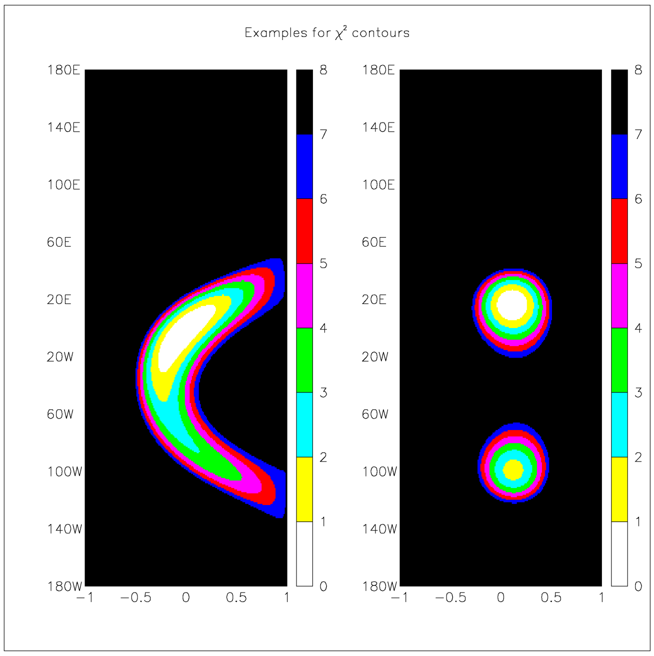

Figure 26: χ^2-contors of reconstructed supernova direction for a randomly choosen supernova event. It was assumed, that timing data from a detector at the South Pole are combined with data from Superkamiokande and SNO. In the left figure, a time resolution of 14 ms (AMANDA-II) was assumed, in the right figure, a time resolution of 3 ms (ICECUBE). The nominal supernova direction was $\cos\theta = 0.1$, $\phi = 2.98$. Note the twofold ambiguity which even for IceCube necessarily remains if only three sites contribute.

9 Summary

The main goal of the IceCube project is the identification of extraterrestrial sources of high energy neutrinos.

- IceCube will reach a sensitvitiy for diffuse fluxes of a few $10^{-9} \cdot E^{-2}$ GeV^{-1} cm^{-2} s^{-1}, which is more than one order of magnitude below conservative upper bounds derived from cosmic ray observations, and three orders of magnitude below bounds derived from gamma ray observations alone. The existing Amanda limit improved previous experimental limits by more than a factor 10 and will be improved by IceCube by additional 2.5 orders of magnitude. Various models predict between several events and a few thousand events per year.
- Point source searches will reach a sensitivity of at least 10^{-12} cm^{-2} s^{-1} for energies greater than 1 TeV. This is nearly two orders of magnitude below the observed Mk501 flux during its flaring phase. Predictions for some steady or quasi-steady sources reach a few ten events per year.
- Supernova models predict 10-100 events shortly before and after the SN burst.
- Gamma Ray Bursts are expected to yield 10-100 events per year.
- IceCube has also significant EeV capabilities. Event numbers predicted by top-down scenarios (like topological defects) lead to 1-30 events per year, comparable to expectations for dedicated EeV experiments.
- IceCube has a realistic chance to identify tau neutrinos via "double-bang" events, with up to 100 events per year expected for certain topological defect models.

IceCube is a multi-purpose detector. Beside high energy neutrino astronomy, it can be used to investigate a series of other questions:

- Magnetic monopoles: Present limits for the flux of relativistic monopoles can be improved by two orders of magnitude. This is a factor of 1000 below the Parker limit. One also can search for slow monopoles catalyzing proton decay, or for strange quark matter.
- Neutrinos from WIMP annihilation: IceCube can play a complementary role to future direct detection experiments, particularly for high WIMP masses.
- MeV neutrinos from supernova bursts: IceCube will detect a possible supernova burst over the whole Galaxy and likely as far as the Magellanic clouds.
- As a by-product, neutrino oscillations, physics with downward muons, or even questions of glaciology can be investigated.

However, being a detector hundred times larger than Amanda and thousand times larger than underground detectors, IceCube will hopefully keep the promise for any detector opening a new window to the Universe: to detect phenomena *not* mentioned in the list above.

References

[1] http://www-zeuthen.desy.de/nuastro/publications/others/proposal.shtml

[2] http://www.ssec.wisc.edu/a3ri/icecube/proposal/

[3] http://www-zeuthen.desy.de/nuastro/ **A-II proposal!**

[4] *The Origin of Cosmic Rays*, V.L. Ginzburg & S.I. Syrovatskii (Pergamon Press, 1964).

[5] M. Nagano *et al.* J. Phys. G10 (1984) 1295.

[6] Yu. A. Fomin *et al.*, Proc. 22nd Int. Cosmic Ray Conf. (Dublin) vol. 2 (1991) 85.

[7] M. Takeda *et al.*, Phys. Rev. Lett. 81 (1998) 1163.

[8] M.A. Lawrence, R.J.O. Reid & A.A. Watson, J. Phys. G17 (1991) 733.

[9] M.I. Pravdin *et al.*, Proc. 26th Int. Cosmic Ray Conf. (Salt Lake City, 1999) vol. 3, p. 292.

[10] D.J. Bird *et al.*, Astrophys. J. 424 (1994) 491.

[11] E.G. Berezhko & H.J. Völk, Astroparticle Phys. 7 (1997) 183.

[12] T.K. Gaisser, F. Halzen, T. Stanev, Phys. Rep. 258 (1995) 173.

[13] E. Waxman & J. Bahcall, Phys. Rev. D 59 (1999) 023002.

[14] G.R. Farrar & T. Piran, Phys. Rev. Letters 84 (2000) 3527.

[15] T. K. Gaisser, to be published in Proceedings of the International Workshop on Observing Ultra-high energy Cosmic Rays from Space and Earth (Metepec, Puebla, Mexico, August 9-12, 2000), astro-ph/0011525.

[16] T.K. Gaisser, Talk given at the OECD Megascience Forum Workshop, Taormina, Sicily, 22/23 May, 1997, astro-ph/9707283.

[17] Mannheim, Protheroe & Rachen, Phys.Rev. D63 (2001) 023003, astro-ph/9812398; J.P. Rachen, R.J. Protheroe & K. Mannheim, Comment presented at the 19th Texas Symposium, Paris, December 1998, astro-ph/9908031.

[18] J. Alvarez-Muñiz and F. Halzen, Phys. Rev. D **63**, 037302 (2001).

[19] L.V. Volkova, Yad. Fiz. **31**, 1510 (1980) [Sov. J. Nucl. Phys. **31**, 784 (1980)].
(1999).

[20] D. Cline and F.W. Stecker, science white paper from UCLA Workshop on High Energy Neutrino Astrophysics, astro-ph/0003459.

[21] R.J. Protheroe and T. Stanev, Phys. Rev. Lett. **77**, 3708 (1996) and Erratum **78**, 3420 (1997).

[22] G. Gelmini and A. Kusenko, Phys. Rev. Lett. **84**, 1378 (2000).

[23] M. Birkel and S. Sarkar, Astropart. Phys. **9**, 297 (1998).

[24] T. Weiler, Astropart. Phys. **11**, 303 (1999); D. Fargion, B. Mele and A. Salis, Astrophys. J. **517**, 725 (1999).

[25] V. Berezinsky, M. Kachelreiß and A. Vilenkin, Phys. Rev. Lett. **79**, 4302 (1997).

[26] F.W. Stecker et al., Phys. Rev. Lett., **66**, 2697 (1991).

[27] J.G. Learned and S. Pakvasa, Astrop. Phys. 3 (1995) pp 267-274.

[28] H. Athar, G. Parente and E. Zas, in preparation.

[29] I.Belolaptikov et al., Astropart.Phys. 7 (1997) 263.

[30] J.Edsjo, WIMP searches with IceCube, Amanda Internal report, Jan.7, 2000.

[31] K.Dick et al., Nucl.Phys. B588 (2000) 101-109 and Nucl.Phys. B598 (2001) 543-553.

[32] Paper in preparation

[33] J.G.Learned, K.Mannheim, High Energy Neutrino Astrophysics, Ann.Rev.Nucl.Phys. (2000).

[34] M.Leuthold, Proc.Simulation and Analysis Methods for Large Neutrino Telescopes, DESY Zeuthen, 1998, DESY-PROC-1999-01 (ed. C.Spiering), 484.

[35] M.Leuthold, IceCube Performance Studies, Amanda Internal Report, Nov.1999.

[36] J.Krabi, C.Spiering et al., preprint PHE 91-03, Zeuthen 1991.

[37] E. Waxman & J. Bahcall, Phys. Rev. D 59 (1999) 023002.

[38] C.Hettlage and K.Mannheim, to appear in the Proceedings of the XXIst Moriond Workshop 'Very High Energy Phenomena in the Universe', Les Arcs, France, January 20-27 2001, astro-ph/0103499

[39] Mannheim, Protheroe and Rachen, Phys.Rev. D63:023003, 2001.

[40] T.Gaisser, to be published in Proceedings of the International Workshop on Observing Ultra-high energy Cosmic Rays from Space and Earth (Metepec, Puebla, Mexico, August 9-12, 2000), astro-ph/0011525.

[41] P. L. Biermann *et al.*, Nucl. Phys. Proc. Suppl. 87 (2000) 417, astro-ph/0008063

[42] K. Rawlins, G.Hill, Amanda Internal Report

[43] A.Hillas et al., Astrophys.J. 503, 744.

[44] T.Weekes, to be included in proceedings of the International Symposium on High Energy Gamma-Ray Astronomy, Heidelberg, June 2000, astrop-ph/0010431.

[45] K.Wang et al., A survey of the Northern sky for TeV point sources, astro-ph/0103353

[46] M.Leuthold, C.Spiering, H.Wissing, Amanda Internal Report.

[47] G.Feldman, J.Cousins, Phys.Rev. D57 (1998) 3873.

[48] S.Barwick, HENAP meeting (Venice, Feb. 2001), Amanda collaboration meeting in March 2001.

[49] S.Hundertmark, Amanda collaboration meeting in Oct. 2000.

[50] P.Meszaros and E.Waxman, astro-ph/0103275.

[51] D.Guetta, Review talk, to appear in the Proc. of the XXIst Rencontres de Moriond "Very High Energy Phenomena in the Universe", Les Arcs, France, Jan. 20-27 (2001), astro-ph/0104045.

[52] C.Schuster, M.Pohl, R.Schlickeiser, Neutrinos from AGN as diagnostic tool, submitted to A&A

[53] E.Waxman, submitted to PRL, astro-ph/0102317.

[54] T.Weiler, submitted to Astro. Part. Phys, astro-ph/0001233.

[55] D.Bakari et al., hep-ex/0004019.

[56] G.Giacomelli and L.Patrizii, Lecture at the Fifth School on Non-Accelerator Particle Astrophysics, Trieste, 29 June - 10 July 1998, hep-ex/0002032.

[57] E.Andres et al., Astropart.Phys.13 (2000) 1.

[58] see report on neutrino analysis on Zeuthen IceCube webpage.

[59] C.Spiering, Nucl.Phys.Proc.Suppl. 91 (2000) 445-452.

[60] L.Köpke and C.Weinheimer, Amanda Internal report.

[61] see K.Scholberg, Nucl.Phys.Proc.Suppl. 91 (2000) 331-337.